Informatics in Medicine Unlocked 29 (2022) 100911

Contents lists available at ScienceDirect

Informatics in Medicine Unlocked

journal homepage: www.elsevier.com/locate/imu

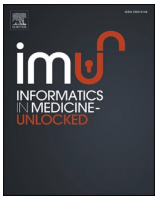

Impact of quality, type and volume of data used by deep learning models in the analysis of medical images

Andreea Roxana Luca [a,b], Tudor Florin Ursuleanu [a,c,d,*], Liliana Gheorghe [a,e,**], Roxana Grigorovici [a], Stefan Iancu [a], Maria Hlusneac [a], Alexandru Grigorovici [a,c]

[a] Faculty of General Medicine, "Grigore T. Popa" University of Medicine and Pharmacy, Iasi, Romania
[b] Integrated Ambulatory of Hospital "Sf. Spiridon", Departament Obstetrics and Gynecology, Iasi, Romania
[c] "Sf. Spiridon" Hospital, Department of Surgery VI, Iasi, Romania
[d] Regional Institute of Oncology, Iasi, Departament of Surgery I, Iasi, Romania
[e] "Sf. Spiridon" Hospital, Department of Radiology, Iasi, Romania

ARTICLE INFO

Keywords:
Medical image analysis
Data types
Labels
Deep learning models

ABSTRACT

The need for time and attention given by the doctor to the patient, due to the increased volume of medical data to be interpreted and filtered for diagnostic and therapeutic purposes has encouraged the development of the option to support, constructively and effectively, deep learning (DL) models for applications in the interpretation of medical images. Imaging physicians combine data from different stages and medical experiences, as opposed to DL models that incorporate the same types and modes of artisanal features. Access to big-databased medical imaging can be considered a benefit to the performance of DL models in interpreting medical imaging but similar or superior performance has been achieved with small, multi-feature and well-categorized databases that have improved annotation and labelling. The major contribution of this paper is primarily to highlight the impact of data quality, type and volume used by deep learning models in medical image analysis accompanied by updated characterization of the components of the deep learning process from data to medical applications. Second, it describes the specific correlations between the components of the deep learning process. Finally, it presents problems and directions for future research.

1. Introduction

The medical data most used in medical practice are medical images and for this reason most deep learning algorithms have targeted this category of medical information for the realization of medical applications.

A large number of medical images are stored in open access databases have private databases of some ceding institutions. These medical images are filed in connection with imaging reports or medical video image reports and, along with language processing from natural images, they have a great contribution to image analysis [1]. Annotation and labelling of the medical image, representing data from doctors, used through methods of integration into deep learning models, consumes time and requires specialized knowledge.

The large volume of training data and properly labelled determines the performance of the deep learning modeling in the interpretation of medical images. Because manual image labelling requires time and specialized training, standardized, organized labelling has been used which has the risk of over-labelling with unnecessary information [2].

In the absence of a large amount of data, the problem of over-assembly can be eliminated by adding abandonment. The deep learning model can have increased preformation in these conditions by optimizing a large number of hyper-parameters (size and number of filters, depth, learning rate, activation function, number of hidden layers, etc.) [3].

In medical image analysis the data types have a high variability and can be exemplified by image captures from different regions [4] different types of data included in a phase [5], different types of images [6], data from doctors that has errors and requires time for processing [7], small sample sizes [8].

This paper presents a methodical review of the literature with the objective of carrying out an analysis of the importance of the

* Corresponding author. Faculty of General Medicine, "Grigore T. Popa" University of Medicine and Pharmacy, Iasi, Romania.
** Corresponding author. Faculty of General Medicine, "Grigore T. Popa" University of Medicine and Pharmacy, Iasi, Romania.
E-mail addresses: tudorursuleanu@yahoo.com (T.F. Ursuleanu), lgheorge123@gmail.com (L. Gheorghe).

https://doi.org/10.1016/j.imu.2022.100911
Received 11 May 2021; Received in revised form 7 March 2022; Accepted 7 March 2022
Available online 9 March 2022
2352-9148/© 2022 The Authors. Published by Elsevier Ltd. This is an open access article under the CC BY license (http://creativecommons.org/licenses/by/4.0/).

relationship between the types and characteristics of scientific data and their use of deep learning models in the interpretation of medical images. We have defined a methodology for semi-automating the production of relevant articles and eliminating those with low impact in the scientific community, by applying inclusive and exclusive quality criteria in the fields of medicine and information technology.

The major contribution of this paper is primarily to highlight the impact of data quality, type and volume used by deep learning models in medical image analysis accompanied by updated characterization of the components of the deep learning process from data to medical applications. Second, it describes the specific correlations between the components of the deep learning process. Finally, it presents problems and directions for future research.

2. State of the arts

The current state of performance of deep learning (DL) models and architectures depends on the nature and quality of the data used in their training. This section shows the data types and DL model description and classification according to medical data types used, objectives and performances in medical applications.

2.1. Scientific data and dataset

Artificial neural networks are universal approximations: a relationship between inputs and outputs can be obtained (a model) with a performance that depends on data sets, topologies, training process, etc., being possible to obtain models for any medical information, such as be medical images. Current medical systems are unable to provide information on huge data sets due to limited laws or medical systems. DL models are just correlations of complex formulas between inputs (example: pixels) and outputs (example: disease labels). There is no semantics in a DL classifier for medical images (the model is not an understanding of medical concepts, but only a matrix of numbers. For this reason, it is not possible for DL to replace a doctor, it is just a tool, similar to the old computer assisted diagnostic (CAD) with predefined rules. There is also no federal intrusion and this involves limiting access to medical data due to inefficient systems and can be avoided, for example, by moving models from one center to another, the images will remain in the property center and patient privacy will be protected [9].

Access to big-databased medical imaging can be considered a benefit to the performance of DL models in interpreting medical imaging but similar or superior performance has been achieved with small, multi-feature and well-categorized databases that have improved annotation and labelling.

Big-databased medical imaging requires the following interventions to improve their quality:

- Stratification of data according to certain characteristics,
- Identifying data with low occurrence in databases and eliminating it to avoid introducing “noise” and destabilize the algoritm
- Segmentation of similar data containing extensions (e.g., gender, age, etc.) by creating sub-segments,
- Segmentation of data to define the area of interest, elimination of variations specific to a feature to avoid the data “noise” of the algorithm, annotation of data that requires effort and time from doctors,
- Data labelling.

There are many large-scale and well-annotated data sets, such as ImageNet 1 (over 14 million images tagged in 20 k categories) and COCO 2 (with over 200 images annotated in 80 categories), medical datasets (open source), such as ChestX-ray14 and Deep-Lesion containing medical images tagged over 100k, the others, contain only a few thousands or even hundreds of medical images, and medical applications have developed properly in the medical fields.

The knowledge of experienced clinical-imaging physicians (radiologists, ophthalmologists and dermatologists, etc.) follows certain characteristics in images, namely, contrast, color, appearance, topology, shape, edges, etc., help and are used by deep learning models to perform the main tasks of medical image analysis [9],10].

The type and volume of medical data, the labels, the category of field knowledge and the methods of their integration into the DL architectures implicitly determine their performance in medical applications [9].

CT, PET-CT, MRI, X-rays, Ultrasound, Diagnostic Biopsy, Mammography and Spectrography are the most used imaging and exploratory investigations in the process of image interpretation, in the objective of extracting characteristics reducing or enlarging the size, in the group, segmentation and classification of images and by using integration methods contribute to the performance of deep learning models, see Fig. 1 [9–12].

Larger datasets, compared to the small size of many medical datasets, result in better deep learning models [4]. The large and well-annotated data sets are: ImageNet, COCO 2, (open source) medical data sets, see Fig. 2.

Acronyms: MRI Magnetic Resonance Images, CT Computed Tomography, SLO Scanning Laser Ophthalmoscopy images, The Alzheimer’s disease neuroimaging initiative (ADNI), Automated cardiac diagnosis challenge (ACDC), The autism brain imaging data exchange (ABIDE), Automated Gleason grading of Prostate cancer tissue-histology images (AGPH) [13], Grand challenge on Breast Cancer Histology images (BACH) [14], Hospital-scale chest x-ray database and benchmarks on weakly-supervised classification and localization of common thorax diseases (Chestx-ray14), The lung image database consortium (LIDC) and image database resource initiative (IDRI) (LIDC-IDRI), Algorithms for automatic detection of pulmonary nodules in computed tomography images (LUNA16), Large dataset for abnormality detection in musculoskeletal radiographs (MURA), Machine learning algorithms for brain tumor segmentation, progression assessment, and overall survival prediction in the brats challenge (BraTS2018), Locating blood vessels in retinal images (STARE), Digital database for screening mammography (DDSM), Automated mining of large-scale lesion annotations and universal lesion detection with deep learning (DeepLesion), Cardiac Magnetic Resonance Images (Cardiac MRI), International skin imaging collaboration (ISIC).

The knowledge of experienced clinical-imagists, follows certain characteristics in images, namely, contrast, color, appearance, topology, shape, edges, etc., It contributes to the performance of medical image interpretation through the use of deep learning models like, anomaly detection models by identifying the characteristics in the image; image segmentation models; image reconstruction models; models for combining two different images into one [15].

The knowledge of imaging doctors can be classified as follows:

1. Low-level medical data
   - Areas of attention of physicians in medical images [16].
   - Disease characteristics [17].
2. High-level medical data
   - Labels – Diagnostic pattern [18],
3. Diagnostic training model that represents specific data identified by doctors [19].

The type and volume of medical data, the labels, the category of field knowledge and the methods of their integration into the DL architectures implicitly determine their performance in medical applications [9].

2.2. Types of data and datasets

We will further expose, the types of images and medical data used for diagnosis: natural images, medical images, high-level medical data

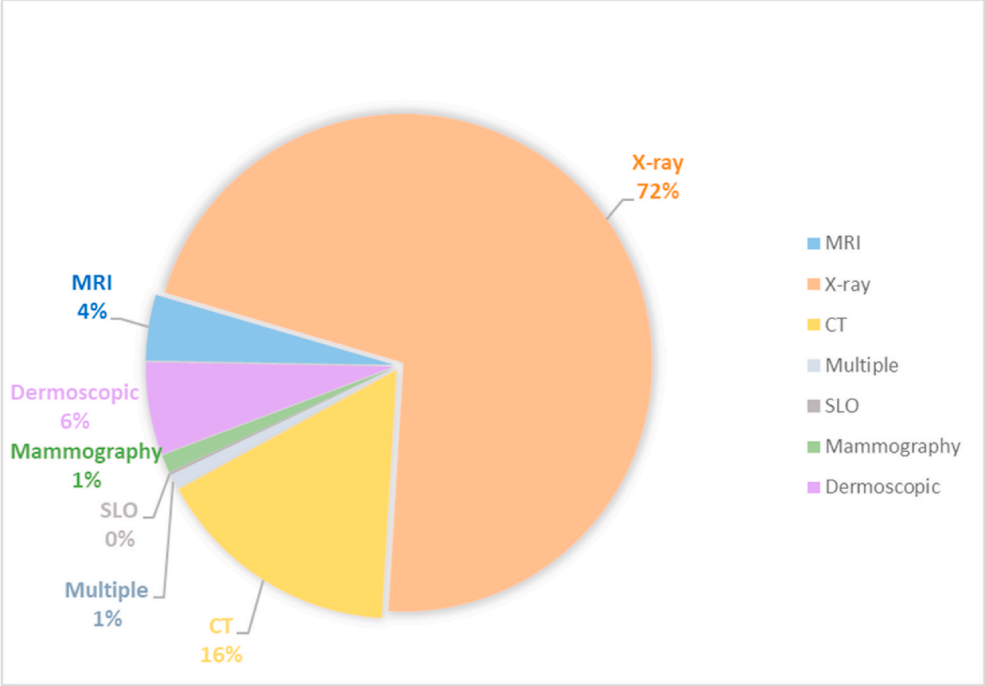

Fig. 1. Imaging and exploratory investigations in the process of image interpretation
Acronyms: MRI Magnetic Resonance Images, CT Computed Tomography, SLO Scanning Laser Ophthalmoscopy images, X-ray on weakly-supervised classification and localization of common thorax diseases [9,10].

(diagnostic pattern), low-level medical data (areas of images, disease characteristics), manual features used for medical image analysis.

2.2.1. Natural images – from natural datasets, ImageNet 1 (over 14 million images tagged in 20k categories) and COCO 2 (with over 200 images annotated in 80 categories). Large natural images (ImageNet) are incorporated for the detection of objects in the medical field and are used in applications for the detection of lymph nodes [20], detection of polyp and pulmonary embolism [21], detection of breast tumors [22], detection of colorectal polyps [23,24]. Natural Images, ImageNet, PASCAL VOC "static data" set, Sports-1M video datasets, which is the largest video classification indicator with 1.1 million sports videos in 487 categories [25].

2.2.2. Medical images from external medical datasets of the same diseases in similar ways (e.g., SFM and DM) [26], medical images from external medical datasets of the same diseases in different ways (DBT and MM, ultrasound) [27] or from different diseases [28]. Medical images are used in multiple applications. Multi-modal medical images, PET images are incorporated for the detection of lesions in CT scans of the liver [29]. Multimodal medical images are also used in another model in the detection of liver tumors [30]. Multimodal medical images (mammographic data) are used to detect breast masses [31]. Medical images, (CT, MRI, angio-CT bottom of the eye images), annotated retinal images, used to help segment the heart vessel without annotations [32]. External medical data and images of other diseases, such as the union dataset (3DSeg-8) by aggregating eight sets of 3D medical segmentation data [33].

2.2.1. Medical data from doctors: high-level medical data (diagnostic pattern) and low-level medical data (areas of images, disease characteristics)

High-level and low-level medical data: anatomical aspects of the image, shape, position, typology of lesions integrated into segmentation tasks, example of the ISBI 2017 dataset used in skin injury segmentation. The use of additional medical datasets in different ways has also proven to be useful, although most applications are limited in using MRI to help segmentation tasks in CT images [34]. Specific data identified by doctors (attention maps, hand-highlighted features) increase the diagnostic performance of deep learning networks (no comparative studies have been conducted). Medical data from doctors, handmade features, handcrafted features, invariant LBP, as well as H & Components, are computed first from the images. The use of the BRATS2015 data set in applications in which these features are used is achieved performance in image segmentation by input-level fusion. However, anatomical priorities are only suitable for segmentation of fixed-shaped organs such as the heart or lungs [33].

2.2.4. Manual features used for medical image analysis is a series of measurements (X-ray projections in CT or spatial frequency information in MRI). The methods based on deep learning have been widely applied in this area [35,36]. Examples: image reconstruction with optical diffuse tomography (DOT), reconstruction of magnetic resonance imaging by compressed detection (CS-MRI) [37], reconstruction of the image with diffuse optical tomography (DOT) of limited-angle breast cancer and limited sources in a strong scattering environment [38], recovery of brain MRI images, target contrast using GAN [39]. Content-based image recovery (CBIR) can be great help to for the clinicians to navigate these large data sets. Some deep learning methods adopt transfer learning to use knowledge from natural images or external medical datasets [40–42], for example, metadata such as age and sex of patients, characteristics extracted from health areas, decision values of binary traits and texture traits in the process of thoracic X-ray recovery.

Medical data used to generate medical reports, subtitling medical images, templates from radiologist reports, visual characteristics of medical images, generating reports using the IU-RR dataset.

2.3. Addressing label noise in the formation of deep learning patterns in medical image analysis

The noise of the label in the formation of deep learning models is important in their performance for medical image analysis. The approach of the label noise was achieved by: cleaning and preprocessing labels, improving the network architecture with noise layer, the endowment of networks with loss functions, data re-

Imaging	Number of Images	Type	Purpose	Name Datasets
Multiple	1921 patients	Brain Breast Prostate Lung	Classification Segmentation	ADNI BACH AGPCH
MRI	539 patients and 573 controls	Brain	Classification	ABIDE
MRI	150 patients	Cardiac	Classification	ACDC
X-ray	112,120 images from 30,805 patients	Chest	Detection	Chest X-ray14
CT X-ray	1018 patients	Lung	Detection	LIDC-IDRI
CT	888 images	Lung	Detection	LUNA16
X-ray	40,895 images from 14,982 patients	Musculo-skeletal	Detection	MURA
MRI	542 images	Brain	Segmentation	BraTS2018
SLO	400 images	Eye	Segmentation	STARE
Mammography	2500 patients	Breast	Classification Detection	DDSM
CT	32,735 images from 4427 patients	Multiple	Classification Detection	DeepLesion
MRI	7980 images from 33 cases	Cardiac	Calssification Segmentation	Cardiac MRI
Dermoscopic	13,000 images	Skin	Classification Detection Segmentation	ISIC 2018

Fig. 2. Types of images datasets in the medical domain.

weighting, data and label consistency, training procedures.

2.3.1. Cleaning and pre-processing labels

In chest X-ray scans in the classification of thoracic diseases, the smoothing of labels was used to handle noisy labels and led to improvements of up to 0.08 in the area below the characteristic receptor operating curve (ASC) [43].

2.3.2. Network architectures

In the case of network architectures, the noise layer proposed by Ref. [44] improved the accuracy in detecting breast lesions in mammograms.

2.3.3. Loss functions

The enhancement of networks with loss functions that cause annotations to dilate with a small and large structuring element to generate noisy masks for the foreground and background, e.g., parts of the ring union image were marked as unsafe regions that were ignored during training [45].

2.3.4. Re-weighting data

Re-weighting of data to cope with noisy annotations in cancer detection was achieved by training models on a large group of noisy label patches using calculated features from a small set of clean label patches and increased model performance by 10% [46]. This strategy was used to classify skin lesions in noisy label images [47], for segmentation of the heart, clavicles and lung in chest X-rays [7], for segmenting the skin lesion from highly inaccurate annotations [48] proposed a specific characteristic of pixels.

2.3.5. Consistency of data and labels

For segmentation of the left atrium in the MRI from tagged and un-labelled data it was proposed to form two separate models: a teacher model that produced noisy labels and labelled maps with non-certainties on un-labelled images and a student model that was trained using the noisy labels generated, while taking into account the uncertainty of the label and making correct predictions on the clean data set in accordance with the teacher's model on the label, with uncertainty below the threshold.

2.3.6. Training procedures

For segmentation of the bladder, prostate and rectum in MRI, a model was trained on a clean label data set and used it to predict segmentation masks for a separate set of un-labelled data, and a second model was instructed to estimate a confidence map to indicate regions where predicted labels were more likely to be accurate and reliable paper used to sample the main model with a 3% improvement in the Dice similarity coefficient (DSC) [49]. A rather similar method has been used to classify aortic valve defects in MRI [50].

2.4. DL model description and classification according to medical data types used, objectives and performances in medical applications

We will synthesize in Fig. 3, Classification of DL models according to the characteristics and tasks for which they were designed, classification of DL models according to the characteristics and tasks for which they were designed [9,10].

DL architectures can be divided into three categories:

Supervised DL models:

- Recurrent Neural Network (RNN): Long-short-term memory (LSTM), Gated Recurrent Unit (GRU),
- Convolutive Neural Network (CNN),
- Generative Adversarial Network (GAN).

Unsupervised deep learning models:

- Deep Network of Beliefs (DBN),
- Deep Transfer Network (DTN),
- Tensor Deep Stack Networks (TDSN),
- Autoencoders (AE).

2.4.1. Below we describe the DL models

CNN (convolutive neural network): CNNs are popular in areas where the shape of an object is an important feature, such as image analysis [15,51–54], particularly in the study of cancers and bodily injuries in the medical sector [55,56] and video analysis [57].

We present in the following considerations on training data and learning categories specific to CNN:

- classification data by level of medical information,
- classification-training on medical iterations,
- hierarchical learning,
- representative learning,
- stratified learning optimization of network parameter,
- optimization of network parameters.

The convolutional neural network (CNN) goes through several stages in the classification of medical images, namely, learning to extract non-informative patches and identify non-informative patches through multiple instances.

CNN contains convolutional layers, grouping layers, dropout layers, and an output layer, hierarchically positioned that each learn stun specific characteristics in the image [58].

CNN in image analysis has low performance when high-resolution datasets are considered [59] and when localization over large patches

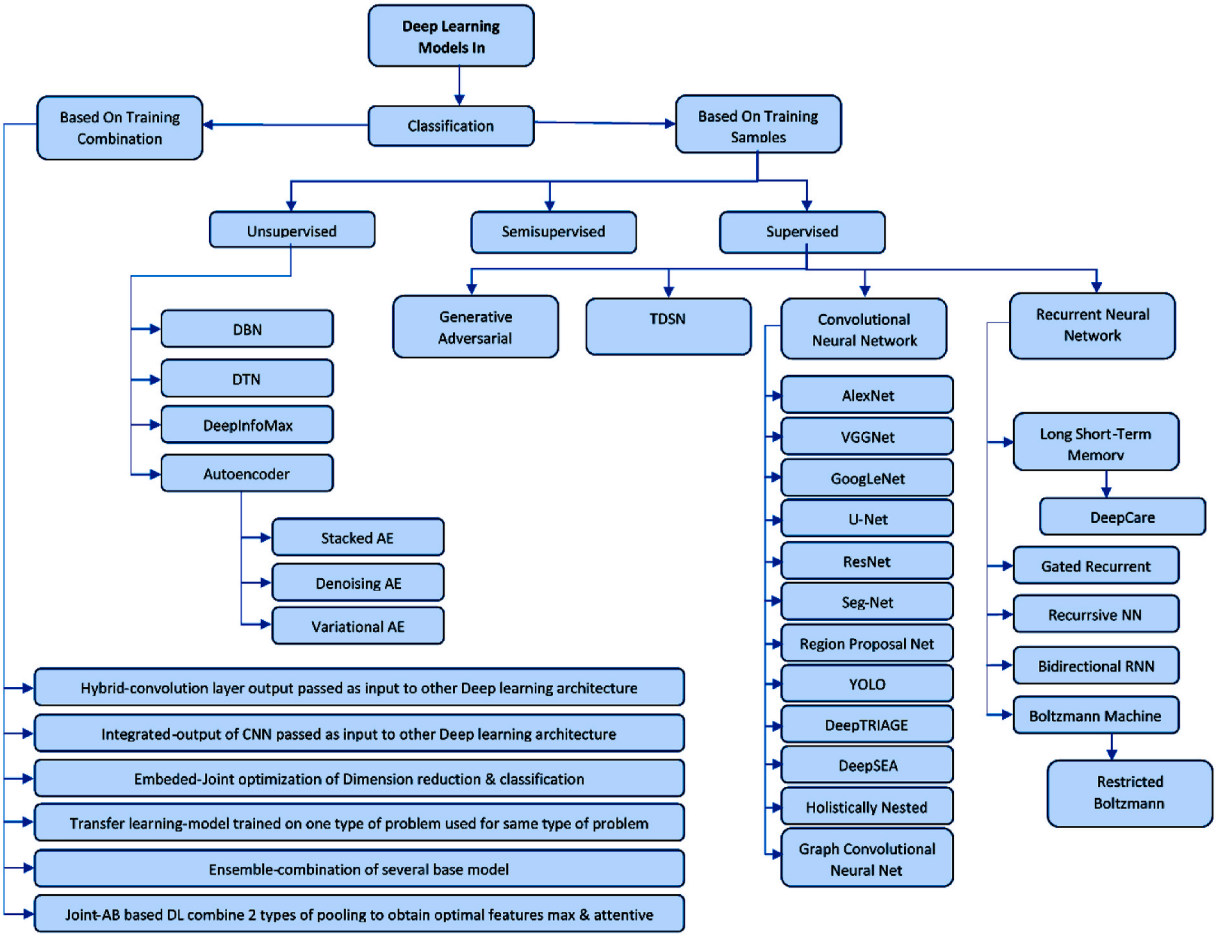

Fig. 3. Classification of DL models according to the characteristics and tasks for which they were designed. Acronyms: Deep Network of Beliefs (DBN), Deep Network of Distribution and Target, Deep Info Max (DIM), AutoEnconder (AE), Generative Adversarial Network (GAN), Tensor Deep Stacking Network (TDSN), Convolutional Neural Network (CNN), Visual Geometry Group Network (VGG Net), Deep Layers Network (GoogLeNet), Fully Convolutional Network (U-Net), Residual Neural Network (ResNet), Deep Segmentation-Emendation Network (SegNet), Region Proposal Net (RPN), You Only Look Once (YOLO), Deep Triage (DT), deep learning–based algorithmic framework (DeepSEA), Holistically-Nested Edge Detection (HED), Graph Convolutional Natural Net (GCNN),Recurent Neuronal Network (RNN), Deep Dynamic Neural Network (Deep Care),Gated Recurrent Network (GRN), Recurrsive RNN(RvNNs), Long Short-Term Memory (LSTM), Bidirectional RNN (BRNN), Restricted Boltzmann Machine (RBM).

is required, especially in medical images [60].

Image analysis performance is enhanced by the use of the following architectures: AlexNet, VGGNet and ResNet, YOLO or U-net that we describe below:

AlexNet was proposed by Refs. [56,57] for the ImageNet Large Scale Visual Recognition Challenge (ILSVRC) in 2012.

AlexNet consists of 8 layers, 5 layers of convolution and 3 dense, fully connected layers, overlapping overlay, abandonment, data augmentation, ReLU activations after each convolutional layer and fully connected, SGD with impulse [56]. AlexNet is used for image recognition in image analysis and is usually applied to issues involving semantic segmentation and high-resolution data classification tasks [61,62].

VGG (Visual Geometry Group): Consists of 13 convolution layers (in VGG16) & 16 convolution layers (in VGG19), 3 dense layers, pooling and three RELU units, very small responsive fields [63]. VGG is used for object recognition, classification of medical images [64,65] and image segmentation [66]. VGG loses accuracy when the depth becomes too high.

ResNet (Residual Neural Network): Contains closed units or closed recurring units and has a strong similarity to recent successful elements applied in RNNs. ResNet is characterized by: residual mapping, identity function; and a two-layer residual block; One layer learns from the residue, the other layer learns from the same function and has high level of performance in image classification (Saravanan et al., Saravanan) and audio analysis tasks [67].

GoogLeNet is built from 22 deep LAYERS CNN and 4 million parameters and contains several layer filters and stacked convolution layers [68]. It was used for batch normalization, image distortions, and RMSprop.

U-Net, developed by Ronneberger [69]. It addresses the problem of locating images of a standard CNN by extracting data features followed by reconstruction of the original dimension through an up-sampling operation. U-Net is a type of Enconder-Decoder network in which the codoficator output belongs to the input space. U-Net is used in single-stage segmentation and classification [70], specifically in the location of cancerous lesions [71–73]. SegNet [74] is a U-Net variant that uses maximum grouping indices in the upsampling step that reduces the complexity of U-Net space.

U-Net-based models:

U-Net [69] and its derivatives segment the medical image with good results. U-Net is based on the FCN structure, consisting of a series of downscaling and upscaling layers and with skip connections between paired convolutional layers in the encoder. U-Net and its variants such as UNet ++ [75] and recurrent U-Net [76] perform well in many medical image segmentation tasks [77–79].

Next, we will present and describe the U-Net-based architectures:

- Attention U-Net - Usually for a segmentation task there is only a part or a few parts of the image that are relevant for the problem. However, the basic U-Net is not capable of focusing on a specific region of interest and that results in excessive processing of irrelevant areas, see Fig. 4.
- KiU-Net - Classical U-Net performs poorly in detecting small structures and does not segment boundaries of regions precisely. This happens because the deeper we go in the

layers of the network, the larger the receptive field is, and this results in a reduced attention to details. A solution to this drawback came with the development of the KiU-Net in 2020 in Ref. [80]. The architecture consists of two networks, a Kite-Net and a U-Net that run in parallel having their results combined, see Fig. 5.

Since Kite-Net alone is only focusing on extracting small structures and the dataset could have both large and small regions to be segmented, it has been put together with U-Net, which performs well at segmenting high-level features, large regions.

- HarDNet - This architecture has been described in Ref. [81] and it has achieved the state-of-the-art on two datasets so far. It appeared as a solution to the failure of U-Net at segmenting small blurry areas, to the lack of coverage for broken image areas and the time-consuming training. It consists of a HarDNet encoder and a partial decoder, which reduces the training time. The encoder is based on a DenseNet but has significantly less connections for cutting computation costs and smaller channel width in order to recover the accuracy lost from connection pruning. The HarDNet block used in encoder is shown in Fig. 6., as an evolution from DenseNet Block. The figure and its description are taken entirely from the original paper [81], see Fig. 6.

U-Net will be enhanced by having a context aggregation block encoder and we will still retain the low-level image features resulting from the U-Net, but we will have slightly finer segmentation of them without adding costs due to context aggregation blocks. Kite-Net will have a unit with attention gates and a Kite-Net decoder, this way we add a benefit of attention to the details of Kite-Net. A partial decoder like the one in the HarDNet-MSEG architecture used as the new U-Net decoder to reduce training time [79].

RNNs were developed by Rumelhart et al. [82] using efficiently the correlations existing between input data of a prediction problem, through which they process sequential data in relation to text analysis [83–85], in electronic medical records to predict diseases [86,87],and

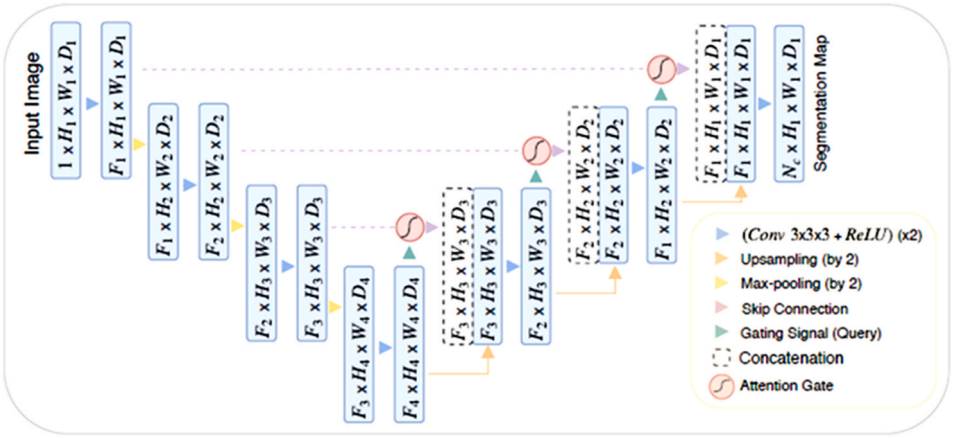

Fig. 4. A block diagram of the proposed Attention U-Net segmentation model. Input image is progressively filtered and down sampled by factor of 2 at each scale in the encoding part of the network (e.g., H4 = H1/8). Nc denotes the number of classes. Attention gates (AGs) filter the features propagated through the skip connections. Feature selectivity in AGs is achieved by use of contextual information (gating) extracted in coarser scales.

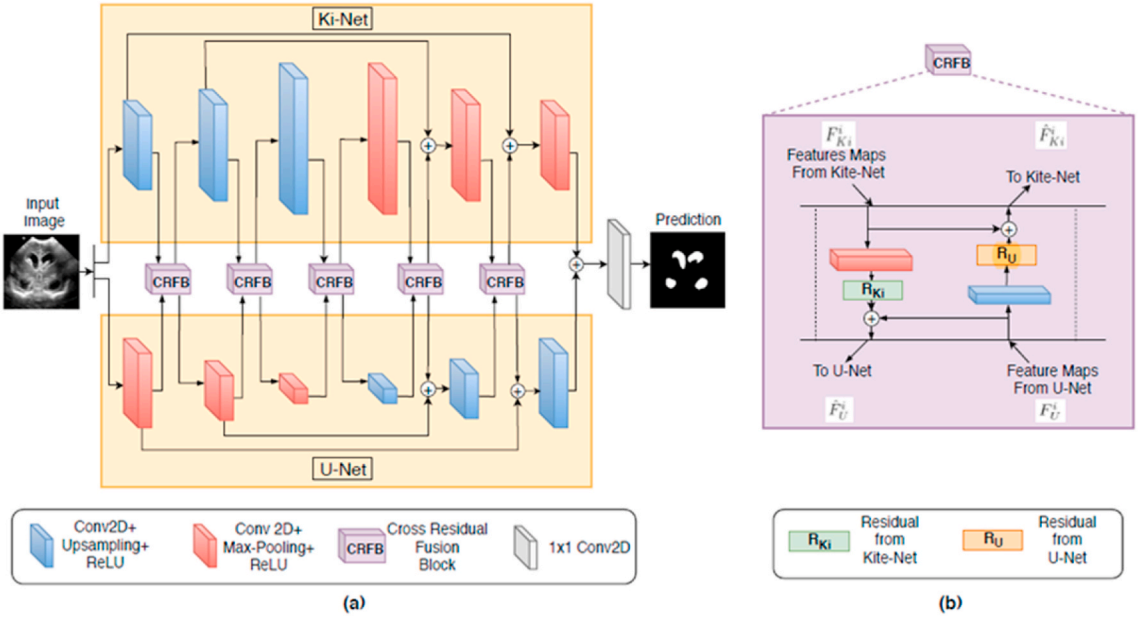

Fig. 5. Architecture details of KiU-Net for 2D image segmentation. In KiU-Net, the input image is forwarded to the two branches of KiU-Net: Kite-Net and U-Net which have CRFB blocks connecting them at each level. The feature maps from the last layer of both the branches are added and passed through 1x1 2D conv to get the prediction. In CRFB, residual features of Kite-Net are learned and added to the features of U-Net to forward the complementary features and vice-versa. (b) Details of Cross Residual Fusion Block (CRFB).

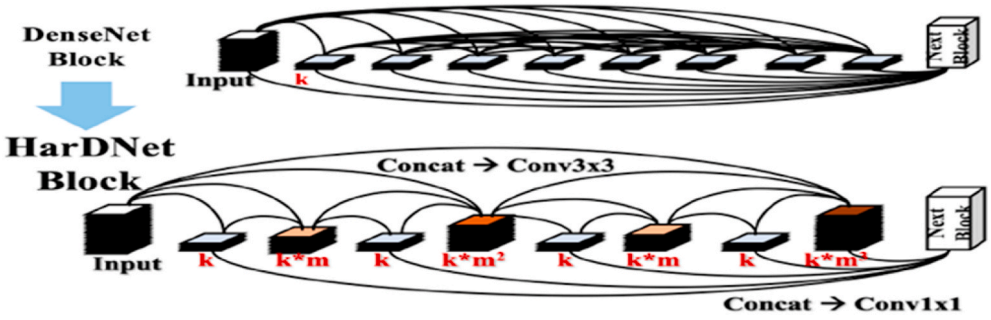

Fig. 6. HarDNet Block overview.

speech recognition [88]. RnN variants are: one-way, learning from the past and predicting the future and bidirectional that uses the future to restore the past. RNN has the following variants: long short-term memory (LSTM) and gated recurring units (GRU), recursive neural networks (Recursive NNs), two-way RNNs (BiRNN). Long-short-term memory LSTMs were introduced by Refs. [65,89] and consist of: the gate of oblivion that alleviates the escape and explosion gradient, the entrance gate and the exit gate, the last two track the flow of data coming in and out of the cell. They were used in speech recognition [90], path prediction [91]and medical diagnosis [92], in which the authors proposed an LSTM network, called DeepCare, combining different types of data to identify clinical diseases.

GRUs (gated recurring unit) created by Refs. [93,94] solve the problem of increasing the time complexity of LSTM, when large amounts of data are used. The GRU consists of a reset gate in which it is decided how much information from the past is transmitted in the future, and an update gate that decides how much information from the past can be forgotten. GRU and LSTMs have similar applications especially in speech recognition [95].

The two-way recurring neural network and the Boltzmann BRNNs introduced by Refs. [96,97] are characterized by the fact that the hidden state is updated by using past information, as in a classic RNN, and by using information related to future moments. They were applied in handwriting and speech recognition, where they are used to detect missing parts of a sentence in a knowledge of the other words [98,99].

BM models, introduced by Refs. [100,101], are a family of RNNs that are easy to implement and that reproduce many probability distributions, BMs are used in image classification. BMs combined with other models are used to locate object [102,103]. In the classification of images, BMs are used to identify the presence of a tumor [104]. BM models are slow and ineffective when the data size increases exponentially due to the complete connection between neurons [104]. A restricted BM was proposed in which relaxing the connections between neurons of the same or one-way connection between neurons would solve the problem of the classic BM model [105].

AEs, developed by Refs. [82,106], consisting of encoder and decoder, have the aim of reducing the size of the data through significant representations and learning data characteristics for the reconstruction of outputs. They are used in applications in medical image analysis [107], natural language processing [108] and video analysis [109].

Additional variants of AE that can be found in the literature are variational AE (VAE). In a VAE, the encoder is represented by the probability density function of the input into the feature space and, after the encoding stage, a sampling of the new data using the PDF is added. Differently from the DAE and the SAE, a VAE is not a regularized AE, but is part of the generation class.

GAN: It is used to generate synthetic training data from original data using a latent distribution [110]. It consists of two networks, a generator that produces a synthetic data, and a discriminator, which differentiates fake data from real data and separates it in order to increase the quality of the data generated. GAN has two problems: the problem of the collapse of the mode, and the fact that, can become very unstable.

DBN (Deep Network of Beliefs), created by Hinton [111], consists of two networks that build each other: of beliefs represented by an acyclic graph composed of layers of stochastic binary units with weighted and respectively weighted connections, restricted Boltzmann Machines which is a stochastic. DBNs are applied in image recognition and speech recognition, in classification to detect lesions in medical diagnosis and, in video recognition to identify the presence of persons [112], in speech recognition to understand missing words in a sentence [113] and in application on physiological signals to recognize human emotion [114].

DTN contains a characteristic extraction layer, which teaches a shared feature subspace in which marginal source distributions and target samples are drawn close and a layer of discrimination that match conditional distributions by classified transduction [115]. It is used for large-scale problems.

TDSN contains two parallel hidden representations that are combined using a bilinear mapping [116]. This arrangement provides better generalization compared to the architecture of a single module. The prejudices of the generalizers with regard to the learning set shall be inferred. It works effectively and better than an eco-validation strategy when used with multiple generalizers compared to individual generalizers.

Deep InfoMax (DIM): Maximizes mutual information between an input and output of a highly flexible convolutional encoder [117] by forming another neural network that maximizes a lower limit on a divergence between the marginal product of encoder input and output. Estimates obtained by another network can be used to maximize the reciprocal information of the features in the input encoder. The memory requirement of the DIM is lower because it requires only encoder not decoder.

2.4.2. Combinations of different DL models depending on the type of data involved in the problem to be solved

DL models can be combined in five different ways depending on the type of data involved in the problem to be solved. Of these, three types of HA (hybrid architectures), namely the integrated model, the built-in model and the whole model [9,10].

In the integrated model, the output of the convolutional layer is transmitted directly as input to other architectures to the residual attention network, the recurrent convolutional neural network (RCNN) and the model of the recurrent residual convolutive neural network (IRRCNN) [118].

In the built-in model (the improved common hybrid CNNBiLSTM), the size reduction model and the classification model perform together, the results of one represent the inputs for the other model. In the model (EJH–CNN–BiLTM), several basic models are combined.

In the transfer learning model (TL) is trained and uses the same type of problem. CNN models that use the TL model are VGG (e.g., VGG16 or VGG19), GoogLeNet (e.g., InceptionV3), Inception Network (Inception-v4), Recurrent Neural Network (e.g., ResNet50), AlexNet. Joint AB based DL combines max pooling, and careful sharing.

2.4.3. Combinations of different DL models to benefit from the characteristics of each model with medical applications are: CNN + RNN, AE + CNN and GAN + CNN

CNN + RNN are used for the capabilities of the CNN feature extraction model and the RNNs [119]. Because the result of a CNN is a 3D value and an RNN works with 2D-data, a remodeling layer is, associated between CNN and RNN, to convert THE production of CNN into an array. CNN + RNN have been successfully applied in text analysis to identify missing words [120] and image analysis to increase the speed of magnetic resonance image storage [121,122]. CNN + RNN variants are obtained by replacing the Standard RNN component with an LSTM component [22,123].

The AE + CNN architecture combines AE as a pre-training model when using data with high noise levels, and a CNN as a feature extractor model. AE + NVs have an application in image analysis to classify noisy medical images [124] and in the reconstruction of medical images [125,126].

GAN + CNN combines GAN as a pre-workout model to moderate the problem of over-mounting, and a CNN, used as a feature extractor. It has applications in image analysis [8,127].

The DL architectures applied especially in image analysis are CNN, AE and GAN. NVs preserve the spatial structure of the data, and are used as feature extractors (especially U-Net), AEs reduce the characteristics of complex images in the analysis process, and GANs are pre-training architectures that select input categories to control overfitting.

3. Applications in medicine and the performance of DL models depending on the therapeutic areas in which they were used

We further highlight the acquisitions in the study of deep learning and its applications in the analysis of the medical image, between 2017 and 2020. You can easily identify references to image labelling and annotation, developing new deep learning models with increased performance, and new approaches to medical image processing:

- diagnosis of cancer by using CNN with different number of layers [128],
- studying deep learning optimization methods and applying in the analysis of medical images [129],
- development of techniques used for endoscopic navigation [130],
- highlighting the importance of data labelling and annotation and knowledge of model performance [131,132],
- perfecting the layer-wise architecture of convolution networks [133], lesson the cost and calculation time for processor training [134],
- description of the use of AI and its applications in the analysis [133] of medical images [135],
- diagnosis in degenerative disorder using deep learning techniques [136]and,
- detection of cancer by processing medical images using the medium change filter technique [137],
- classification of cancer using histopathological images and highlighting the rapidity of Theano, a superior variant of Tensor flow [137],
- development of two-channel computational algorithms using DL (segmentation, extraction of characteristics, selection of characteristics and classification and classification, extraction of high-level captures respectively) [138],
- malaria detection using a deep neural network (MM-ResNet) [5,10].

We will exemplify in Table 1 [139] applications in medicine and the performance of DL models depending on types of medical images and the therapeutic areas in which they were used. We included most relevant papers about the most used medical investigations, respectively medical images.

4. Conclusions

Doctors interpret images descriptively (contour, contrast, appearance, localization, etc.) by using data from different excipients and successive stages in the analysis of medical images. These handcrafted features consume time and do not have a standardized character.

Data quality and volume, annotations and labels, identification and automatic extraction of specific medical terms can help deep learning models perform in the tasks of image analysis. Incorporating these

Table 1
Applications and the performances of the DL models depending on the types of medical images and the therapeutic area.

	Type Of Data	Sample	Objective	Model Design	Results	Therapeutic Area	Paper
Mammography	Mammography images	45,000 images	Detect malign solid lesions and prevent overtreatment in false positives	CNN	AUC of 0.90	Oncology	[103]
	Mammography	667 benign and 333 malignant	Mammography diagnosis of early malignant breast	Stacked AE	Accuracy of 0.89	Oncology	[102]
	Digital Mammography images and the biopsy result of the lesions	1000 malignant masses and 600 cysts images and theirs biopsy	CAD to discriminate benign cysts from malignant masses	CNN	AUC of 0.80	Oncology	[103]
	Mammography images	840 images of mammograms from 210 different patients	Breast arterial calcification on mammograms classifier to evaluate the risk of coronary disease	CNN	Misclassified cases of 6%	Cardiovascular	[106]
	Digital mammograms	661 from 444 patients	Computer automated estimation of breast percentage density	CNN	AUC of 0.981	Oncology	[140]
	Mammography images	Mammograms from 604 women	Segment areas of dense fibro-glandular tissue in the breast	CNN	Accuracy of 0.66	Oncology	[121]
	Digital mammograms images	29,107 left mediolateral oblique, right mediolateral oblique, left cranial-caudal and right cranial-caudal mammograms images	Probability of cancer on mammograms	CNN	AUC of 0.90	Oncology	[126]
	Type Of Data	Sample	Objective	Model Design	Results	Therapeutic Area	Paper
Ultrasound	Ultrasound image of the heart 2D	400 images with five different heart diseases and 80 normal echocardiogram images	Segment left ventricle images with greater precision	Deep belief networks	Hammoude distance of 0.80	Cardiovascular	[141]
	Ultrasound imaging	306 malignant and 136 benign tumors images	CAD system to detect and differentiate breast lesions with ultrasound	CNNs inspired in AlexNet, U-Net and ResNet	Best F-measure of 0.91 and 0.89 depending on the data	Oncology	[22]
	Transesophageal ultrasound volume and 3D geometry of the aortic valve images	3795 vol from the aortic valves from 150 patients	Diagnose, stratification and treatment planning for patients with aortic valve pathologies	Marginal space deep learning	Position error of 1.66 mms and mean corner distance error of 3.29 mms	Cardiovascular	[90]
Radiography	Radiography images	7821 subjects with 6 monitoring phases	CAD for diagnosis of knee osteoarthritis	Deep Siamese	Accuracy of 0.66	Traumatology	[120]
	Radiography images	420 radiography images (219 control group, 201 osteoarthritis)	Radiographies CAD for hip osteoarthritis diagnosis	CNN	Accuracy of 0.92	Traumatology	[142]
	Radiographs	112,120 frontal views chest radiographs from 30,805 patients and 17,202 frontal view chest radiographs with a binary class label for normal vs abnormal	Abnormality detection in chest radiographs	CNN	AUROCs of 0.960 and 0.951. AUROCs of 0.900 and 0.893	Radiology	[143]
	Type Of Data	Sample	Objective	Model Design	Results	Therapeutic Area	Paper
Slide image	Pathology cancer images (hematoxylin and eosin)	5202 images tumor infiltrating Lymphocytes	Study of tumor tissue samples. Localize areas of necrosis and lymphocyte infiltration	Two CNNs	AUC of 0.95	Oncology	[144]
	H&E colored tissue	Images with over 21,000 annotated nuclear borders	Segmentation technique	CNNs	Accuracy of 0,92	Diseases of multiple organs	[145]
	Giemsa-stained thin blood smear slides cell images	27,558 cell images 150 infected and 50 healthy patients	Create a screening system for Malaria	CNN	Accuracy of 0.94	Infectious Disease	[86]
	Microscopy image patches	249 images belonging to 20 histologic categories	Classification of breast cancer histology microscopy images	CNN with a Support Vector Machine (SVM)	Accuracy of 0.77 for four class classification and an accuracy of 0.83 for carcinoma/non-carcinoma classification	Oncology	[113]
	Microscopy histopathological images	7909 images of eight subclasses of breast cancers	CAD for breast cancer histopathological diagnosis	CNN	Accuracy of 0.93	Oncology	[114]
	Microscope images	200 female subjects aged from 22 to 64	Cervix cancer screening	Multiscale CNN	Mean and standard deviation of 0.95 and 0.18	Oncology	[127]

(*continued on next page*)

Table 1 (*continued*)

	Type Of Data	Sample	Objective	Model Design	Results	Therapeutic Area	Paper
	Whole-slide prostate histopathology images	2663 images from 32 whole slide prostate histopathology images	Whole-slide histopathology images to outline the malignant regions	CNN	Dice coefficient of 0.72	Oncology	[146]

	Type Of Data	Sample	Objective	Model Design	Results	Therapeutic Area	Paper
Ocular fundus	2D Ocular fundus images	243 retina images	Diagnose retinal lesions	CNN	Precision recall curve of 0.86 in microaneurysms and 0.64 in exudates	Ophthalmology	[84]
	Ocular fundus images 2D	Over 85,000 images	Diabetic retinopathy detection and stage classification	Bayesian CNN	AUC value of 0.99	Ophthalmology	[94]
	Color ocular fundus images	6679 random sampling images from Kaggle's Diabetic Retinopathy Detection	Detect retinal hemorrhages	CNN	AUC of 0.894 and 0.972	Ophthalmology	[101]
	Ocular fundus images	168 images with glaucoma and 428 control	System to detect and evaluate glaucoma	CNN: ResNet and U-Net	AUC of 0.91 and 0.84 respectively	Ophthalmology	[147]
	Ocular fundus images	90,000 images with their diagnoses	Predict the evolution of diabetic retinopathy with fundus images	CNN	AUC of 0.95	Ophthalmology	[148]
	Fundus images	7000 color fundus images	Image quality in the context of diabetic retinopathy	CNN	Accuracy of 100%	Ophthalmology	[149]
	AREDS (age related eye disease study) image	130,000 fundus images	Diagnosis of Age-related Macular Degeneration	CNN	94.97 sensitivity and 98.32% specificity	Ophthalmology	[138]
	Fundus images	219,302 from normal participants without hypertension, diabetes mellitus (DM), and any smoking history	Predict age and sex from retinal fundus images	CNN	AUC 0.96	Ophthalmology	[150]

	Type Of Data	Sample	Objective	Model Design	Results	Therapeutic Area	Paper
Dermoscopy	Dermoscopy images	350 images of melanomas and 374 benign nevus	Dermoscopy CAD system for acral lentiginous melanoma diagnosis	CNN	Accuracy of over 0.80	Oncology	[104]
	Patient demographics and clinical images	49,567 images	Recognize nails nychomycosis lesions	Region-based-CNN	AUC of 0.98, AUC of 0.95, AUC of 0.93, AUC value of 0.82 in the different datasets	Dermatology	[125]
	Stress 99mTc-sestamibi or tetrofosmin myocardial perfusion images	1638 patients	Obstructive coronary disease automatic prediction system	CNN	Sensitivity value of 0.82 and 0.69 for both use cases	Cardiovascular	[151]
Arterial labelling	Arterial spin labelling (ASL) perfusion images	140 subjects	Monitoring cerebral arterial perfusion via spin labelling	CNN	AUC of 0.94	Cardiovascular	[97]
Frames from endoscopy	Frames from endoscopy videos	205 normal and 360 abnormal images	Detection and localization system of gastrointestinal anomalies via endoscopy	CNN	AUC of over 0.80	Gastroenterology	[107]
Tracking dataset multi-instrument Endo-Visceral Surgery and multi-instrument in vivo	Single-instrument Retinal Microsurgery Instrument Tracking dataset, Multi-instrument Endo-Visceral surgery and multi-instrument in vivo images	940 frames of the training data (4479 frames) and 910 frames for the test data (4495 frames)	Detect the two-dimensional position of different medical instruments in endoscopy and microscopy surge	Convolutional Detection regression network	Accuracy of 0.94	Robotic Surgery	[124]

	Type Of Data	Sample	Objective	Model Design	Results	Therapeutic Area	Paper
CT/PET-CT/ SPECT	Nuclear MRIs 3D	124 double echo steady state from 17 patients	Diagnose possible soft tissue injuries	Deep-Resolve, a 3D-CNN model	MSE of 0.008	Traumatology	[152]
	Retinal 3D images obtained by Optical Coherence Tomography	269 patients with AMD, 115 control patients	Retina age-related macular degeneration diagnostic	CNN	AUC of 0	Ophthalmology	[83]
	123I-fluoropropyl carbomethoxyiodophenyl nortropane single-photon emission computed tomography (FP-CIT SPECT) 2D images	431 patient cases	Automatic interpretation system in Parkinson's disease	CNN	Accuracy of 0.96	Neurology-Psychiatry	[85]

(*continued on next page*)

Table 1 (*continued*)

	Type Of Data	Sample	Objective	Model Design	Results	Therapeutic Area	Paper
	Abdominal CT 3D images	231 computed abdominal tomographies	CAD system to classify tomographies and evaluate the malignity degree in gastro-intestinal stromal tumors (GISTs)	Hybrid system between convolutional networks and radiomics	AUC of 0.882	Oncology	[153]
	CT image patches 2D	14,696 images from 120 patients with proven diagnose	CAD system to diagnose interstitial lung disease	CNN	Accuracy of 0.85	Pneumology	[91]
	3D MRI and PET	93 Alzheimer Disease, 204 MCI Mild Cognitive Impairment converters and normal control subjects	CAD for early Alzheimer disease stages	Multimodal DBM	Accuracy of 0.95, 0.85 and 0.75 for the three use cases	Neurology-Psychiatry	[99]
	Type Of Data	Sample	Objective	Model Design	Results	Therapeutic Area	Paper
MRI	Diffusion-weighted imaging maps using MRI	222 patients. 187 treated with rtPA (recombinant tissue-type plasminogen activator)	Decide Acute Ischemic Stroke patients' treatment through volume lesions prediction	CNN	AUC of 0.88	Neurology-Psychiatry	[53]
	Magnetic resonance images	474 patients with schizophrenia and 607 healthy subjects	Schizophrenia detection	Deep discriminant autoencoder network	Accuracy over 0.8	Neurology-Psychiatry	[55]
	Gadoxetic acid–enhanced 2D MRI	144,180 images from 634 patients	Staging liver fibrosis through MR	CNN	AUC values of 0.84, 0.84, and 0.85 for each stage	Gastroenterology	[59]
	Resting state functional magnetic resonance imaging (rs-fMRI), T1 structural cerebral images and phenotypic information	505 individuals with autism and 520 matched typical controls	Identify different autism spectrum disorders	Denoising AE	Accuracy of 0.70	Neurology-Psychiatry	[64]
	3D MRI and PET	93 Alzheimer Disease, 204 MCI Mild Cognitive Impairment converters and normal control subjects	CAD for early Alzheimer disease stages	Multimodal DBM	Accuracy of 0.95, 0.85 and 0.75 for the three use cases	Neurology-Psychiatry	[65]
	Type Of Data	Sample	Objective	Model Design	Results	Therapeutic Area	Paper
CT/PET-CT/ SPECT	12 categories of medical diagnostic images, such as CT images, MRI images and PET images, and 18 categories of illustrations	6776 images for training and 4166 for tests	Classify medical diagnostic images according to the modality they were produced and classify illustrations according to their production attributes	CNN and a synergic signal system	Accuracy of 0.86	Various	[112]
	CT image 2D	63,890 patients with cancer and 171,345 healthy	Discriminate lung cancer lesions in adenocarcinoma, squamous and small cell carcinoma	CNN	Log-Loss error of 0.66 with a sensitivity of 0.87	Oncology	[123]
	CT 2D images	3059 images from several parts of human body	Speed up CT images collection and rebuild the data	DenseNet and a deconvolution model	RMSE of 0.00048	Various	[8]
	CT images 3D	6960 lung nodule regions, 3480 of which were positive samples and rest were negative samples (non-nodule)	CAD to diagnose lung cancer in low-dosage computed tomography	Eye-tracking sparse attentional model and convolutional neural network	Accuracy of 0.97	Oncology	[154]
	CT images 2D and text (reports)	9000 training and 1000 testing images	Processing text from CT reports in order to classify their respective images	CNN	Accuracy of 0.95, 0.70 and 0.58 respectively for the three use cases	Various	[155]
	Computed tomography (CT)	Three datasets: 224,316, 112,120 and 15,783	Binary classification of posteroanterior chest x-ray	CNN	92% accuracy	Radiology	[156]

	Type Of Data	Sample	Objective	Model Design	Results	Therapeutic Area	Paper
MRI	Clinical characteristics and MRI 3D	135 patients with short-, Medium and long-term survival	Predict the survival of patients with amyotrophic lateral sclerosis	CNN	Accuracy of 0.84	Neurology-Psychiatry	[108]
	Optical coherence tomography images	52,690 AMD patients' images and 48,312 control	Differentiate Age-Related Macular Degeneration lesions in optical coherence tomography	Modification of VGG16 CNN	AUC of 0.92, AUC of 0.93 and AUC of 0.97 for the different use cases	Ophthalmology	[109]
	Lung computed axial tomography 2D images and breast ultrasound lesions	520 breast sonograms from 520 patients (275 benign and 245 malignant lesions) and lung CT image data from 1010 patients (700 malignant and 700 benign nodules)	CAD system to classify breast ultrasound lesions and lung CT nodules	Stacked denoising AE	AUC of 0.94	Oncology	[157]
	MRI 2D	444 images from 195 patients with prostate cancer	CAD to prevent errors in diagnosing prostate	CNN	AUC of 0.94	Oncology	[158]
	MRI 2D	MICCAI 2009 left ventricle segmentation challenge database	Determinate limits between the endocardium and epicardium of the left ventricle	RNN with automatic segmentation techniques	Accuracy of 1.0 in the best case	Cardiovascular	[111]

	Type Of Data	Sample	Objective	Model Design	Results	Therapeutic Area	Paper
MRI	12 categories of medical diagnostic images, such as CT images, MRI images and PET images, and 18 categories of illustrations	6776 images for training and 4166 for tests	Classify medical diagnostic images according to the modality they were produced and classify illustrations according to their production attributes	CNN and a synergic signal system	Accuracy of 0.86	Various	[112]
	12 patients' and 14 patients' CT and MRI images	12 patients' pelvic data and 14 patients' brain data	Generation of pseudo-CT using MRI imaging for potential treatment with MRI-based radiotherapy planning.	CNN	Accuracy of 0,98 and 0,95	Brain and Pelvic	[159]
	Functional MRI	68 subjects perform 7 activities, and a state of rest	Analyze cerebral cognitive functions	3D CNN, resting state networks	Accuracy of 0.94	Neurology-Psychiatry	[119]
	Liver MRIs	522 liver MRI cases with and without contrast for known or suspected liver cirrhosis or focal liver lesion	Screening system for undiagnosed hepatic magnetic resonance images	CNN	Reduces negative predictive value and leads to greater precision	Gastroenterology	[122]
	MRI images	1064 brain images of autism patients and healthy controls. MRI data from 110 multiple sclerosis patient	Automatically evaluate the quality of multicenter structural brain MRI images	CNN	AUC 0.90 and 0.71	Radiology	[160]

Acronyms: AMD age-related Macular Degeneration, CAD Computer Aided Diagnosis, CNN Convolutional Neural Network, MRI Magnetic Resonance Images, PET Photon Emission Tomography, CT Computed Tomography, OCT Optical Coherence Tomography, D dimensions, AUC Area Under the Curve, MSE Mean Squared Error, RMSE Root Mean Square Error, DSC Dice Similarity Coefficient.

features, labels, into DL architectures increases their performance.

High-level domain knowledge is incorporated as input images, and low-level domain knowledge is learned using specific network structures [33] and, together with direct networking, low-level domain knowledge information can also be used to design training commands when combined with the easy-to-use training model [161].

DL can be a support in solving complex problems of interpretation of medical images and provides the doctor with support in making medical decisions and time for patient care.

Imaging doctors combine data from different stages and experiences as opposed to DL models that incorporate the same types and modes of handcrafted features. Data quality and volume, annotations and labels, identification and automatic extraction of specific medical terms can help deep learning models perform in the tasks of image analysis [9,77].

5. Research problems

Problems in medical image analysis can be categorized as follows:

- Identification, automatic extraction and standardization of specific medical terms,
- Representation of medical knowledge,
- Incorporation of medical knowledge.

Problems in medical image analysis are related to:

- Medical images provided as data for deep-street models require: quality, volume, specificity, labelling.
- Providing data from doctors, descriptive data, labels are ambiguous for the same medical and non-standard references
- Laborious time in data processing are problems to solve in the future.
- Lack of clinical trials demonstrating the benefits of using DL medical applications in reducing morbidity and mortality and improving patient quality of life [9,10,162–164].

Luca AR et. all., presents the problems and approaches of using deep learning applications in medicine by highlighting, classifying the emotions, feelings and attitudes of physicians in the practical interaction with AI, providing an aesthetic experience in their color palette (emotions and feelings).

The holistic approach to the doctor-patient-AI relationship is the solution to in-creasing the attention and involvement of doctors in the use of high-performance technologies for support in medical practice. Compliance with performance criteria, ethics, active involvement through knowledge and technology performance in the realization of the medical act can increase the acceptance of doctors in working with AI and implicitly the good results of medical practice with the aim of increasing the quality of life of patients.

6. Future challenges

In traditional machine learning, the common learning process is separated and is carried out only on certain models, data sets and tasks. Therefore, knowledge is not retained or transferred to each other models. Instead, in deep learning, transfer learning can use knowledge such as the weights and characteristics of a pre-trained model to prepare a new model, as well as to address problems in the Roman task that has a smaller amount of data. Transfer learning with deep learning patterns is faster, has improved accuracy and/or needs less training data [9,165].

A new approach to transfer learning, to address the problem of lack of data training in medical imaging tasks is represented by the technique of learning by transfer called dual transfer learning.

We use the learned features to improve the performance of other tasks, such as classification in skin lesions, benign and malignant or in the case of breast lesions classification of breast histological images into four classes: invasive carcinoma, in situ carcinoma, benign tumor and normal tissue [9,166].

These consist of adapting the domain consisting of transferring data from one domain to another domain by using labels; knowledge graph characterized by the incorporation of multimodal medical data; generating models capable of extracting features unsupervised and easily incorporated into the architecture of DL networks; techniques to search for a particular network architecture according to the defined objectives data [9,10].

The adaptation of the domain consisted of transferring information from a source domain to a target domain, such as adversarial learning [167], and makes it restrict the domain change between source and target domain in input space [168], feature space [169,170], and output space [171,172]. It can be used to transfer knowledge about one set of medical data to another [173], even when they have different modes of imaging or belong to different disease [174,175]. UDA (unsupervised domain adaptation), which uses medical labels, has demonstrated performance in disease diagnosis and organ segmentation [143,173,176,177].

The knowledge graph has the specifics of incorporating multimodal medical data and achieves performance in medical image analysis and the creation of medical reports [178]. The graphs of medical knowledge describing, the relationship between different types of knowledge, the relationship between different diseases, the relationship between medical datasets and a type of medical data, help deep learning models work [179].

Generativ models, GAN ~~and AE~~ are mainly used for segmentation activities. GAN uses MRI datasets to segment CT images [175,176]. GAN is a type of unsupervised deep learning network used in medical image analysis. AE are used in extracting features, shape priorities in objects such as organs or lesions, completely unsupervised and are easily incorporated into the network formation process [33,180].

Network Architecture Search Technique (NAS) can automatically identify a specific network architecture in computer tasks [181] and promises that utility and performance in the medical field [182].

Funding

Scientific research funded by the University of Medicine and Pharmacy “Gr. T. Popa” of Iasi, based on contract number 4714.

Declaration of competing interest

The authors declare that they have no known competing financial interests or personal relationships that could have appeared to influence the work reported in this paper.

Acknowledgments

Dr. Tudor Florin Ursuleanu, Dr. Andreea Roxana Luca and Prof. Dr. Alexandru Grigorovici is thankful to UMF Iasi-Romania grant no 4714/2021 (UMF), Romania under which the current research work was carried out.

References

[1] Shin HC, Lu L, Summers RM. natural language processing for large-scale medical image analysis using deep learning. Deep Learn. Med. Image Anal. Jan. 2017: 405–21. https://doi.org/10.1016/B978-0-12-810408-8.00023-7.

[2] Wang X, Yang X, Dou H, Li S, Heng P-A, Ni D. Joint segmentation and Landmark localization of fetal femur in ultrasound volumes. 2019 IEEE EMBS Int Conf Biomed Heal Informatics BHI 2019 - Proc Aug. 2019. Aug. 07, 2021. [Online]. Available: https://arxiv.org/abs/1909.00186v1.

[3] Ravi D, et al. Deep learning for health informatics. IEEE J Biomed Heal Informatics Jan. 2017;21(1):4–21. https://doi.org/10.1109/JBHI.2016.2636665.

[4] Sharma S, Mehra R. Conventional machine learning and deep learning approach for multi-classification of breast cancer histopathology images—a comparative insight. J Digit Imag Jan. 2020;33(3):632–54. https://doi.org/10.1007/S10278-019-00307-Y. 2020 333.

[5] Pattanaik PA, Mittal M, Khan MZ, Panda SN. Malaria detection using deep residual networks with mobile microscopy. J. King Saud Univ. - Comput. Inf. Sci. Jul. 2020. https://doi.org/10.1016/J.JKSUCI.2020.07.003.

[6] He Y, et al. DPA-DenseBiasNet: semi-supervised 3D fine renal artery segmentation with dense biased network and deep priori anatomy. In: Lecture Notes in computer science (including subseries lecture Notes in artificial Intelligence and lecture Notes in bioinformatics). 11769. LNCS; 2019. p. 139–47.

[7] Zhu Y, Tong L, Deshpande SR, Wang MD. Improved prediction on heart transplant rejection using convolutional autoencoder and multiple instance learning on whole-slide imaging. 2019 IEEE EMBS Int. Conf. Biomed. Heal. Informatics May 2019. https://doi.org/10.1109/BHI.2019.8834632. BHI 2019 - Proc..

[8] Zhang Z, Liang X, Dong X, Xie Y, Cao G. A sparse-view CT reconstruction method based on combination of DenseNet and deconvolution. IEEE Trans Med Imag Jun. 2018;37(6):1407–17. https://doi.org/10.1109/TMI.2018.2823338.

[9] Ursuleanu TF, et al. Deep learning application for analyzing of constituents and their correlations in the interpretations of medical images. Diagnostics Jul. 2021; 11(8):1373. https://doi.org/10.3390/DIAGNOSTICS11081373. 2021.

[10] Ursuleanu TF, et al. Unified analysis specific to the medical field in the interpretation of medical images through the use of deep learning. E-Health Telecommun Syst Netw Jun. 2021;10(2):41–74. https://doi.org/10.4236/ETSN.2021.102003.

[11] Salvi M, Acharya UR, Molinari F, Meiburger KM. The impact of pre- and post-image processing techniques on deep learning frameworks: a comprehensive review for digital pathology image analysis. Comput Biol Med 2021;128(Jan). https://doi.org/10.1016/J.COMPBIOMED.2020.104129.

[12] Lee J-G, et al. Deep learning in medical imaging: general overview. Korean J Radiol Aug. 2017;18(4):570–84. https://doi.org/10.3348/KJR.2017.18.4.570.

[13] Arvaniti E, et al. Automated Gleason grading of prostate cancer tissue microarrays via deep learning. Sci Rep Aug. 2018;8(1):1–11. https://doi.org/10.1038/s41598-018-30535-1. 2018 81.

[14] Aresta G, et al. BACH: Grand challenge on breast cancer histology images. Med Image Anal Aug. 2019;56:122–39. https://doi.org/10.1016/J.MEDIA.2019.05.010.

[15] Lundervold AS, Lundervold A. An overview of deep learning in medical imaging focusing on MRI. Z Med Phys May 2019;29(2):102–27. https://doi.org/10.1016/J.ZEMEDI.2018.11.002.

[16] Tan J, Huo Y, Liang Z, Li L. Expert knowledge-infused deep learning for automatic lung nodule detection. J Xray Sci Technol Jan. 2019;27(1):17–35. https://doi.org/10.3233/XST-180426.

[17] Majtner T, Yildirim-Yayilgan S, Hardeberg JY. Combining deep learning and hand-crafted features for skin lesion classification. In: 2016 6th Int. Conf. Image process. Theory, tools appl. IPTA 2016; Jan. 2017. https://doi.org/10.1109/IPTA.2016.7821017.

[18] Hussein S, Cao K, Song Q, Bagci U. Risk stratification of lung nodules using 3D CNN-based multi-task learning. Lect Notes Comput Sci (including Subser Lect Notes Artif Intell Lect Notes Bioinformatics) 2017;10265:249–60. https://doi.org/10.1007/978-3-319-59050-9_20. LNCS.

[19] Liu W, et al. SSD: single shot MultiBox detector. Lect Notes Comput Sci (including Subser Lect Notes Artif Intell Lect Notes Bioinformatics) 2016;9905:21–37. https://doi.org/10.1007/978-3-319-46448-0_2. LNCS.

[20] Shin HC, et al. Deep convolutional neural networks for computer-aided detection: CNN architectures, dataset characteristics and transfer learning. IEEE Trans Med Imag May 2016;35(5):1285–98. https://doi.org/10.1109/TMI.2016.2528162.

[21] Tajbakhsh N, et al. Convolutional neural networks for medical image analysis: full training or fine tuning? IEEE Trans Med Imag May 2016;35(5):1299–312. https://doi.org/10.1109/TMI.2016.2535302.

[22] Yap MH, et al. Automated breast ultrasound lesions detection using convolutional neural networks. IEEE J Biomed Heal Informatics Jul. 2018;22(4):1218–26. https://doi.org/10.1109/JBHI.2017.2731873.

[23] Näppi JJ, Hironaka T, Regge D, Yoshida H. Deep transfer learning of virtual endoluminal views for the detection of polyps in CT colonography', in *Medical Imaging 2016: computer-Aided Diagnosis*. Mar 2016;9785:97852B. https://doi.org/10.1117/12.2217260.

[24] Zhang R, et al. Automatic detection and classification of colorectal polyps by transferring low-level CNN features from nonmedical domain. J Biomed Heal Informatics Jan. 2017;21(1):41–7. https://doi.org/10.1109/JBHI.2016.2635662.

[25] 'Learning spatiotemporal features with 3D convolutional networks. IEEE Conference Publication | IEEE Xplore', https://ieeexplore.ieee.org/document/7410867. [Accessed 7 August 2021].

[26] RK S, Hp C, LM H, MA H, KH C, CD R. Multi-task transfer learning deep convolutional neural network: application to computer-aided diagnosis of breast cancer on mammograms. Phys Med Biol Nov. 2017;62(23):8894–908. https://doi.org/10.1088/1361-6560/AA93D4.

[27] Samala RK, Chan HP, Hadjiiski L, Helvie MA, Richter CD, Cha KH. Breast cancer diagnosis in digital breast tomosynthesis: effects of training sample size on multi-stage transfer learning using deep neural nets. IEEE Trans Med Imag Mar. 2019; 38(3):686–96. https://doi.org/10.1109/TMI.2018.2870343.

[28] Liao Q, Ding Y, Jiang ZL, Wang X, Zhang C, Zhang Q. Multi-task deep convolutional neural network for cancer diagnosis. Neurocomputing Jul. 2019; 348:66–73. https://doi.org/10.1016/J.NEUCOM.2018.06.084.

[29] Ben-Cohen A, et al. Cross-modality synthesis from CT to PET using FCN and GAN networks for improved automated lesion detection. Eng Appl Artif Intell Feb. 2019;78:186–94. https://doi.org/10.1016/J.ENGAPPAI.2018.11.013.

[30] Zhao J, et al. Tripartite-GAN: synthesizing liver contrast-enhanced MRI to improve tumor detection. Med Image Anal Jul. 2020;63:101667. https://doi.org/10.1016/j.media.2020.101667.

[31] Zhang J, Saha A, Zhu Z, Mazurowski MA. Hierarchical convolutional neural networks for segmentation of breast tumors in MRI with application to radiogenomics. IEEE Trans Med Imag Feb. 2019;38(2):435–47. https://doi.org/10.1109/TMI.2018.2865671.

[32] Yu F, et al. Annotation-free cardiac vessel segmentation via knowledge transfer from retinal images. In: Lecture Notes in computer science (including subseries lecture Notes in artificial Intelligence and lecture Notes in bioinformatics). 11765. LNCS; 2019. p. 714–22.

[33] Chen C, Biffi C, Tarroni G, Petersen S, Bai W, Rueckert D. Learning shape priors for robust cardiac MR segmentation from multi-view images. Lect Notes Comput Sci (including Subser Lect Notes Artif Intell Lect Notes Bioinformatics) 2019; 11765:523–31. https://doi.org/10.1007/978-3-030-32245-8_58. LNCS.

[34] Valindria VV, et al. Multi-modal learning from unpaired images: application to multi-organ segmentation in CT and MRI. Proc. - 2018 IEEE Winter Conf Appl Comput Vision, WACV 2018 May 2018;2018-January:547–56. https://doi.org/10.1109/WACV.2018.00066.

[35] Qin C, Schlemper J, Caballero J, Price AN, Hajnal JV, Rueckert D. Convolutional recurrent neural networks for dynamic MR image reconstruction. IEEE Trans Med Imag Jan. 2019;38(1):280–90. https://doi.org/10.1109/TMI.2018.2863670.

[36] Schlemper J, Caballero J, Hajnal JV, Price AN, Rueckert D. A deep cascade of convolutional neural networks for dynamic MR image reconstruction. IEEE Trans Med Imag Feb. 2018;37(2):491–503. https://doi.org/10.1109/TMI.2017.2760978.

[37] Yang G, et al. DAGAN: deep de-aliasing generative adversarial networks for fast compressed sensing MRI reconstruction. IEEE Trans Med Imag Jun. 2018;37(6): 1310–21. https://doi.org/10.1109/TMI.2017.2785879.

[38] Ben Yedder H, Shokoufi M, Cardoen B, Golnaraghi F, Hamarneh G. Limited-angle diffuse optical tomography image reconstruction using deep learning. Lect Notes Comput Sci (including Subser Lect Notes Artif Intell Lect Notes Bioinformatics) Oct. 2019;11764:66–74. https://doi.org/10.1007/978-3-030-32239-7_8. LNCS.

[39] Dar SUH, Yurt M, Shahdloo M, Ildız ME, Çukur T. Synergistic reconstruction and synthesis via generative adversarial networks for accelerated multi-contrast MRI. May 2018. Aug. 05, 2021. [Online]. Available: http://arxiv.org/abs/1805.10704.

[40] Ahmad J, Sajjad M, Mehmood I, Baik SW, 'SiNC. Saliency-injected neural codes for representation and efficient retrieval of medical radiographs. PLoS One Aug. 2017;12(8):e0181707. https://doi.org/10.1371/journal.pone.0181707.

[41] Khatami A, Babaie M, Tizhoosh HR, Khosravi A, Nguyen T, Nahavandi S. A sequential search-space shrinking using CNN transfer learning and a Radon projection pool for medical image retrieval. Expert Syst Appl Jun. 2018;100: 224–33. https://doi.org/10.1016/j.eswa.2018.01.056.

[42] Swati ZNK, et al. Content-based brain tumor retrieval for MR images using transfer learning. IEEE Access 2019;7:17809–22. https://doi.org/10.1109/ACCESS.2019.2892455.

[43] Pham HH, Le TT, Ngo DT, Tran DQ, Nguyen HQ. Interpreting chest X-rays via CNNs that exploit hierarchical disease dependencies and uncertainty labels. Neurocomputing May 2020;437:186–94.

[44] Bekker AJ, Goldberger J. Training deep neural-networks based on unreliable labels. ICASSP, IEEE Int Conf Acoust Speech Signal Process - Proc May 2016; 2016-May:2682–6. https://doi.org/10.1109/ICASSP.2016.7472164.

[45] Matuszewski DJ, Sintorn IM. Minimal annotation training for segmentation of microscopy images. Proc - Int Symp Biomed Imaging May 2018;2018-April: 387–90. https://doi.org/10.1109/ISBI.2018.8363599.

[46] Ren M, Zeng W, Yang B, Urtasun R. Learning to reweight examples for robust deep learning. 35th Int Conf Mach Learn ICML 2018 Mar. 2018;10:6900–9. Aug. 07, 2021. [Online]. Available: https://arxiv.org/abs/1803.09050v3.

[47] Xue C, Dou Q, Shi X, Chen H, Heng PA. Robust learning at noisy labeled medical images: applied to skin lesion classification. Proc - Int Symp Biomed Imaging Jan. 2019;2019-April:1280–3.

[48] Mirikharaji Z, Yan Y, Hamarneh G. Learning to segment skin lesions from noisy annotations. Lect Notes Comput Sci (including Subser Lect Notes Artif Intell Lect Notes Bioinformatics) Jun. 2019;11795:207–15. LNCS.

[49] Nie D, Gao Y, Wang L, Shen D. ASDNet: attention based semi-supervised deep networks for medical image segmentation. Lect Notes Comput Sci (including Subser Lect Notes Artif Intell Lect Notes Bioinformatics) 2018;11073:370–8. https://doi.org/10.1007/978-3-030-00937-3_43. LNCS.

[50] Fries JA, et al. Weakly supervised classification of rare aortic valve malformations using unlabeled cardiac MRI sequences. Aug. 2018. p. 339630. https://doi.org/10.1101/339630. bioRxiv.

[51] Jiang F, et al. Artificial intelligence in healthcare: past, present and future. Stroke Vasc Neurol Dec. 2017;2(4):230–43. https://doi.org/10.1136/SVN-2017-000101.

[52] DD M, EW B. Artificial intelligence in medical practice: the question to the answer? Am J Med Feb. 2018;131(2):129–33. https://doi.org/10.1016/J.AMJMED.2017.10.035.

[53] HJ J, KO C. Applications of deep learning for the analysis of medical data. Arch Pharm Res Jun. 2019;42(6):492–504. https://doi.org/10.1007/S12272-019-01162-9.

[54] Bakator M, Radosav D. Deep learning and medical diagnosis: a review of literature. Multimodal Technol Interact 2018 Aug. 2018;2(3):47. https://doi.org/10.3390/MTI2030047.

[55] Hecht-Nielsen R. Neurocomputing: picking the human brain. IEEE Spectr 1988;25 (3):36–41. https://doi.org/10.1109/6.4520.

[56] Krizhevsky A, Sutskever I, Hinton GE. ImageNet classification with deep convolutional neural networks. Commun ACM Jun. 2017;60(6):84–90. https://doi.org/10.1145/3065386.

[57] Arasu A, Garcia-Molina H, University S. Extracting structured data from Web pages. Proc 2003 ACM SIGMOD Int. Conf Manag 2003:337. https://doi.org/10.1145/872757.872799. data - SIGMOD '03.

[58] Vizcarra J, Place R, Tong L, Gutman D, Wang MD. Fusion in breast cancer histology classification. ACM-BCB 2019 - Proc 10th ACM Int Conf Bioinformatics Comput Biol Heal Informatics Sep. 2019:485–93. https://doi.org/10.1145/3307339.3342166.

[59] Velicer WF, Molenaar PC. 'Time series analysis for psychological research', *Handb. Psychol.* second ed. Sep. 2012. https://doi.org/10.1002/9781118133880.HOP202022.

[60] LeCun Y, et al. Backpropagation Applied to Handwritten Zip Code Recognition. Neural Comput Dec. 1989;1(4):541–51. https://doi.org/10.1162/NECO.1989.1.4.541.

[61] Kipf TN, Welling M. 'Semi-Supervised classification with graph convolutional networks', 5th Int. Conf. Learn. Represent. ICLR 2017 - Conf. Track proc. Sep. 2016. Accessed: Aug. 05, 2021. [Online]. Available: https://arxiv.org/abs/1609.02907v4.

[62] Elman JL. Finding structure in time. Cognit Sci 1990;14(2):179–211. https://doi.org/10.1207/S15516709COG1402_1. Mar.

[63] Simonyan K, Zisserman A. Very deep convolutional networks for large-scale image recognition. 3rd Int Conf Learn Represent ICLR 2015 - Conf Track Proc Sep. 2014. Aug. 05, 2021. [Online]. Available: https://arxiv.org/abs/1409.1556v6.

[64] J. León et al., 'Deep learning for EEG-based motor imagery classification: accuracy-cost trade-off', PLoS One, vol. 15, no. 6, p. e0234178, Jun. 2020, doi: 10.1371/JOURNAL.PONE.0234178.

[65] S. Hochreiter and J. Schmidhuber, 'Long short-term memory', Neural Comput., vol. 9, no. 8, pp. 1735–1780, Nov. 1997, doi: 10.1162/NECO.1997.9.8.1735.

[66] Sathya R, Abraham A. Comparison of supervised and unsupervised learning algorithms for pattern classification. Int J Adv Res Artif Intell 2013;2(2). https://doi.org/10.14569/IJARAI.2013.020206.

[67] Gondara L. Medical image denoising using convolutional denoising autoencoders. IEEE Int Conf Data Min Work ICDMW Jul. 2016:241–6. https://doi.org/10.1109/ICDMW.2016.0041. 0.

[68] Zhou B, Khosla A, Lapedriza A, Torralba A, Oliva A. Places: an image database for deep scene understanding. J Vis Oct. 2016;17(10):296. Aug. 05, 2021. [Online]. Available: https://arxiv.org/abs/1610.02055v1.

[69] Ronneberger O, Fischer P, Brox T. U-net: convolutional networks for biomedical image segmentation. Lect Notes Comput Sci (including Subser Lect Notes Artif Intell Lect Notes Bioinformatics) 2015;9351:234–41. https://doi.org/10.1007/978-3-319-24574-4_28.

[70] Nowling RJ, et al. Classification before segmentation: improved u-net prostate segmentation. In: 2019 IEEE EMBS Int. Conf. Biomed. Heal. Informatics, BHI 2019 - Proc.; May 2019. https://doi.org/10.1109/BHI.2019.8834494.

[71] Pesteie M, Abolmaesumi P, Rohling RN. Adaptive augmentation of medical data using independently conditional variational auto-encoders. IEEE Trans Med Imag Dec. 2019;38(12):2807–20. https://doi.org/10.1109/TMI.2019.2914656.

[72] Yu EM, Iglesias JE, Dalca AV, Sabuncu MR. An auto-encoder strategy for adaptive image segmentation. Proc Mach Learn Res Rev Apr. 2020:1–11. Aug. 07, 2021. [Online]. Available: https://arxiv.org/abs/2004.13903v1.

[73] Uzunova H, Schultz S, Handels H, Ehrhardt J. Unsupervised pathology detection in medical images using conditional variational autoencoders. Int J Comput Assist Radiol Surg Dec. 2018;14(3):451–61. https://doi.org/10.1007/S11548-018-1898-0. 2018 143.

[74] Chen M, Shi X, Zhang Y, Wu D, Guizani M. Deep features learning for medical image analysis with convolutional autoencoder neural network. IEEE Trans. Big Data Jun. 2017:1. https://doi.org/10.1109/TBDATA.2017.2717439. 1.

[75] Zhou Z, Rahman Siddiquee MM, Tajbakhsh N, Liang J. UNet++: a nested U-net architecture for medical image segmentation. Lect Notes Comput Sci (including Subser Lect Notes Artif Intell Lect Notes Bioinformatics) Sep. 2018;11045:3–11. https://doi.org/10.1007/978-3-030-00889-5_1. LNCS.

[76] Zahangir Alom M, Yakopcic C, Taha TM, Asari VK. Nuclei segmentation with recurrent residual convolutional neural networks based U-net (R2U-net). Proc IEEE Natl Aerosp Electron Conf NAECON Dec. 2018;2018:228–33. https://doi.org/10.1109/NAECON.2018.8556686. July.

[77] Xie X, Niu J, Liu X, Chen Z, Tang S, Yu S. A survey on incorporating domain knowledge into deep learning for medical image analysis. Med Image Anal 2021;69:101985. https://doi.org/10.1016/J.MEDIA.2021.101985. Apr.

[78] Gordienko Y, et al. Deep learning with lung segmentation and bone shadow exclusion techniques for chest X-ray analysis of lung cancer. Adv Intell Syst Comput Jan. 2018;754:638–47. https://doi.org/10.1007/978-3-319-91008-6_63.

[79] Luca AR, et al. Designing a high-performance deep learning theoretical model for biomedical image segmentation by using key elements of the latest U-Net-Based architectures. J Comput Commun Jul. 2021;9(7):8–20. https://doi.org/10.4236/JCC.2021.97002.

[80] Valanarasu JMJ, Sindagi VA, Hacihaliloglu I, Patel VM. KiU-net: Overcomplete convolutional architectures for biomedical image and volumetric segmentation. Oct. 2020. Aug. 05, 2021. [Online]. Available: http://arxiv.org/abs/2010.01663.

[81] Huang C-H, Wu H-Y, Lin Y-L, 'HarDNet-MSEG. A simple encoder-decoder polyp segmentation neural network that achieves over 0.9 mean Dice and 86 FPS'. Jan. 2021. Aug. 05, 2021. [Online]. Available: http://arxiv.org/abs/2101.07172.

[82] Rumelhart DE, Hinton GE, Williams RJ. Learning representations by back-propagating errors. Nat 1986;323(6088):533–6. https://doi.org/10.1038/323533a0. 1986 3236088.

[83] Apostolopoulos S, Ciller C, De Zanet SI, Wolf S, Sznitman R. RetiNet: automatic AMD identification in OCT volumetric data. Oct. 2016. Aug. 05, 2021. [Online]. Available: http://arxiv.org/abs/1610.03628.

[84] Lam C, Yu C, Huang L, Rubin D. Retinal lesion detection with deep learning using image patches. Invest Ophthalmol Vis Sci Jan. 2018;59(1):590–6. https://doi.org/10.1167/IOVS.17-22721.

[85] Choi H, Ha S, Im HJ, Paek SH, Lee DS. Refining diagnosis of Parkinson's disease with deep learning-based interpretation of dopamine transporter imaging. NeuroImage Clin 2017;16:586–94. https://doi.org/10.1016/J.NICL.2017.09.010. Jan.

[86] Rajaraman S, et al. Pre-trained convolutional neural networks as feature extractors toward improved malaria parasite detection in thin blood smear images. PeerJ Apr. 2018;6(4):e4568. https://doi.org/10.7717/PEERJ.4568.

[87] Nielsen A, Hansen MB, Tietze A, Mouridsen K. Prediction of tissue outcome and assessment of treatment effect in acute ischemic stroke using deep learning. Stroke 2018;49(6):1394–401. https://doi.org/10.1161/STROKEAHA.117.019740.

[88] Lee H-C, Ryu H-G, Chung E-J, Jung C-W. Prediction of bispectral index during target-controlled infusion of propofol and RemifentanilA deep learning approach. Anesthesiology Mar. 2018;128(3):492–501. https://doi.org/10.1097/ALN.0000000000001892.

[89] Zeng L-L, et al. Multi-site diagnostic classification of schizophrenia using discriminant deep learning with functional connectivity MRI. EBioMedicine Apr. 2018;30:74–85. https://doi.org/10.1016/J.EBIOM.2018.03.017.

[90] Ghesu FC, Georgescu B, Zheng Y, Hornegger J, Comaniciu D. Marginal space deep learning: efficient architecture for detection in volumetric image data. Lect Notes Comput Sci (including Subser Lect Notes Artif Intell Lect Notes Bioinformatics) Oct. 2015;9349:710–8. https://doi.org/10.1007/978-3-319-24553-9_87.

[91] Anthimopoulos M, Christodoulidis S, Ebner L, Christe A, Mougiakakou S. Lung pattern classification for interstitial lung diseases using a deep convolutional neural network. IEEE Trans Med Imag May 2016;35(5):1207–16. https://doi.org/10.1109/TMI.2016.2535865.

[92] Yasaka K, Akai H, Kunimatsu A, Abe O, Kiryu S. Liver fibrosis: deep convolutional neural network for staging by using gadoxetic acid–enhanced hepatobiliary phase MR images287; Dec.2017. p. 146–55. https://doi.org/10.1148/RADIOL.2017171928. 1.

[93] Cho K, et al. Learning phrase representations using RNN encoder-decoder for statistical machine translation. In: Emnlp 2014 - 2014 Conf. Empir. Methods Nat. Lang. Process. Proc. Conf.; Jun. 2014. p. 1724–34. Aug. 07, 2021. [Online]. Available: https://arxiv.org/abs/1406.1078v3.

[94] Leibig C, Allken V, Ayhan MS, Berens P, Wahl S. Leveraging uncertainty information from deep neural networks for disease detection. Sci Rep Dec. 2017;7(1):1–14. https://doi.org/10.1038/s41598-017-17876-z. 2017 71.

[95] Kooi T, et al. Large scale deep learning for computer aided detection of mammographic lesions. Med Image Anal Jan. 2017;35:303–12. https://doi.org/10.1016/J.MEDIA.2016.07.007.

[96] Schuster M, Paliwal KK. Bidirectional recurrent neural networks. IEEE Trans Signal Process 1997;45(11):2673–81. https://doi.org/10.1109/78.650093.

[97] Kim E-K, et al. Applying data-driven imaging biomarker in mammography for breast cancer screening: preliminary study. Sci Rep Feb. 2018;8(1):1–8. https://doi.org/10.1038/s41598-018-21215-1. 2018 81.

[98] Heinsfeld AS, Franco AR, Craddock RC, Buchweitz A, Meneguzzi F. Identification of autism spectrum disorder using deep learning and the ABIDE dataset. NeuroImage Clin Jan. 2018;17:16–23. https://doi.org/10.1016/J.NICL.2017.08.017.

[99] Il Suk H, Lee SW, Shen D. Hierarchical feature representation and multimodal fusion with deep learning for AD/MCI diagnosis. Neuroimage Nov. 2014;101:569–82. https://doi.org/10.1016/J.NEUROIMAGE.2014.06.077.

[100] Hinton G, Vinyals O, Dean J. Distilling the knowledge in a neural network. Mar. 2015. Aug. 05, 2021. [Online], http://arxiv.org/abs/1503.02531.

[101] Van Grinsven MJJP, Van Ginneken B, Hoyng CB, Theelen T, Sánchez CI. Fast convolutional neural network training using selective data sampling: application to hemorrhage detection in color fundus images. IEEE Trans Med Imag May 2016;35(5):1273–84. https://doi.org/10.1109/TMI.2016.2526689.

[102] Wang J, Yang X, Cai H, Tan W, Jin C, Li L. Discrimination of breast cancer with microcalcifications on mammography by deep learning. Sci Rep Jun. 2016;6(1):1–9. https://doi.org/10.1038/srep27327. 2016 61.

[103] Kooi T, van Ginneken B, Karssemeijer N, den Heeten A. Discriminating solitary cysts from soft tissue lesions in mammography using a pretrained deep convolutional neural network. Med Phys Mar. 2017;44(3):1017–27. https://doi.org/10.1002/MP.12110.

[104] Yu C, et al. Correction: acral melanoma detection using a convolutional neural network for dermoscopy images. PLoS One Apr. 2018;13(4):e0196621. https://doi.org/10.1371/JOURNAL.PONE.0196621.

[105] Wong E. Media review: deep medicine: how artificial intelligence can make healthcare human again. InnovAiT Educ Inspir Gen Pract 2021:175573802110182. https://doi.org/10.1177/17557380211018237.

[106] Wang J, et al. Detecting cardiovascular disease from mammograms with deep learning. IEEE Trans Med Imag May 2017;36(5):1172–81. https://doi.org/10.1109/TMI.2017.2655486.

[107] Iakovidis DK, Georgakopoulos SV, Vasilakakis M, Koulaouzidis A, Plagianakos VP. Detecting and locating gastrointestinal anomalies using deep learning and iterative cluster unification. IEEE Trans Med Imag Oct. 2018;37(10):2196–210. https://doi.org/10.1109/TMI.2018.2837002.

[108] van der Burgh HK, Schmidt R, Westeneng HJ, de Reus MA, van den Berg LH, van den Heuvel MP. Deep learning predictions of survival based on MRI in

amyotrophic lateral sclerosis. NeuroImage Clin Jan. 2017;13:361–9. https://doi.org/10.1016/J.NICL.2016.10.008.
[109] Lee CS, Baughman DM, Lee AY. Deep learning is effective for classifying normal versus age-related macular degeneration OCT images. Ophthalmol Retin Jul. 2017;1(4):322–7. https://doi.org/10.1016/J.ORET.2016.12.009.
[110] Hsieh Y-J, Tseng H-C, Chin C-L, Shao Y-H, Tsai T-Y. Based on DICOM RT structure and multiple loss function deep learning algorithm in organ segmentation of head and neck image. IFMBE Proc Apr. 2019;74:428–35. https://doi.org/10.1007/978-3-030-30636-6_58.
[111] Hinton Geoffrey E, Osindero Simon, Teh Yee-Whye. A fast learning algorithm for deep belief nets. Neural Comput 2006;18(7):1527–54.
[112] Zhang J, Xia Y, Wu Q, Xie Y. Classification of medical images and Illustrations in the biomedical literature using synergic deep learning. Jun. 2017. Aug. 05, 2021. [Online]. Available: http://arxiv.org/abs/1706.09092.
[113] Araújo T, et al. Classification of breast cancer histology images using Convolutional Neural Networks. PLoS One Jun. 2017;12(6):e0177544. https://doi.org/10.1371/JOURNAL.PONE.0177544.
[114] Han Z, Wei B, Zheng Y, Yin Y, Li K, Li S. Breast cancer multi-classification from histopathological images with structured deep learning model. Sci Rep Jun. 2017;7(1):1–10. https://doi.org/10.1038/s41598-017-04075-z. 2017 71.
[115] Zhang X, Yu FX, Chang S-F, Wang S. Deep transfer network: unsupervised domain adaptation. Mar. 2015. Aug. 05, 2021. [Online]. Available: http://arxiv.org/abs/1503.00591.
[116] Hutchinson B, Deng L, Yu D. Tensor deep stacking networks. IEEE Trans Pattern Anal Mach Intell 2013;35(8):1944–57. https://doi.org/10.1109/TPAMI.2012.268.
[117] Hjelm RD, et al. 'Learning deep representations by mutual information estimation and maximization', 7th Int. Conf. Learn. Represent. ICLR 2019. Aug. 2018. Aug. 05, 2021. [Online]. Available: https://arxiv.org/abs/1808.06670v5.
[118] Alom MZ, Yakopcic C, Nasrin MS, Taha TM, Asari VK. Breast cancer classification from histopathological images with inception recurrent residual convolutional neural network. J Digit Imag Feb. 2019;32(4):605–17. https://doi.org/10.1007/S10278-019-00182-7. 2019 324.
[119] Y. Zhao et al., 'Automatic recognition of fMRI-derived functional networks using 3-D convolutional neural networks', IEEE Trans Biomed Eng, vol. 65, no. 9, pp. 1975–1984, Sep. 2018, doi: 10.1109/TBME.2017.2715281.
[120] Tiulpin A, Thevenot J, Rahtu E, Lehenkari P, Saarakkala S. Automatic knee osteoarthritis diagnosis from plain radiographs: a deep learning-based approach. Sci Rep Jan. 2018;8(1):1–10. https://doi.org/10.1038/s41598-018-20132-7. 2018 81.
[121] Lee J, Nishikawa RM. Automated mammographic breast density estimation using a fully convolutional network. Med Phys Mar. 2018;45(3):1178–90. https://doi.org/10.1002/MP.12763.
[122] Esses SJ, et al. Automated image quality evaluation of T2-weighted liver MRI utilizing deep learning architecture. J Magn Reson Imag Mar. 2018;47(3):723–8. https://doi.org/10.1002/JMRI.25779.
[123] Serj MF, Lavi B, Hoff G, Valls DP. A deep convolutional neural network for lung cancer diagnostic. Apr. 2018. Aug. 05, 2021. [Online]. Available: http://arxiv.org/abs/1804.08170.
[124] Du X, et al. Articulated multi-instrument 2-d pose estimation using fully convolutional networks. IEEE Trans Med Imag May 2018;37(5):1276–87. https://doi.org/10.1109/TMI.2017.2787672.
[125] Han SS, et al. Deep neural networks show an equivalent and often superior performance to dermatologists in onychomycosis diagnosis: automatic construction of onychomycosis datasets by region-based convolutional deep neural network. PLoS One Jan. 2018;13(1):e0191493. https://doi.org/10.1371/JOURNAL.PONE.0191493.
[126] Kim KH, Choi SH, Park S-H. Improving arterial spin labeling by using deep learning287; Dec. 2017. p. 658–66. https://doi.org/10.1148/RADIOL.2017171154. 2.
[127] Song Y, Zhang L, Chen S, Ni D, Lei B, Wang T. Accurate segmentation of cervical cytoplasm and nuclei based on multiscale convolutional network and graph partitioning. IEEE Trans Biomed Eng Oct. 2015;62(10):2421–33. https://doi.org/10.1109/TBME.2015.2430895.
[128] Haryanto T, Wasito I, Suhartanto H. Convolutional Neural Network (CNN) for gland images classification. In: Proc. 11th Int. Conf. Inf. Commun. Technol. Syst. ICTS 2017. 2018-January; Jan. 2018. p. 55–9. https://doi.org/10.1109/ICTS.2017.8265646.
[129] Cao H, Bernard S, Heutte L, Sabourin R. Improve the performance of transfer learning without fine-tuning using dissimilarity-based multi-view learning for breast cancer histology images. Lect Notes Comput Sci (including Subser Lect Notes Artif Intell Lect Notes Bioinformatics) Jun. 2018;10882:779–87. https://doi.org/10.1007/978-3-319-93000-8_88. LNCS.
[130] Luo X, Mori K, Peters TM. Advanced endoscopic navigation: surgical big data, methodology, and applications, 20; Jun. 2018. p. 221–51. https://doi.org/10.1146/ANNUREV-BIOENG-062117-120917.
[131] Xiao C, Choi E, Sun J. Opportunities and challenges in developing deep learning models using electronic health records data: a systematic review. J Am Med Inf Assoc Oct. 2018;25(10):1419–28. https://doi.org/10.1093/JAMIA/OCY068.
[132] Shickel B, Tighe PJ, Bihorac A, Rashidi P, 'Deep EHR. A survey of recent advances in deep learning techniques for electronic health record (EHR) analysis. IEEE J Biomed Heal Informatics Sep. 2018;22(5):1589–604. https://doi.org/10.1109/JBHI.2017.2767063.
[133] Pandey B, Kumar Pandey D, Pratap Mishra B, Rhmann W. A comprehensive survey of deep learning in the field of medical imaging and medical natural language processing: challenges and research directions. J King Saud Univ - Comput Inf Sci 2021. https://doi.org/10.1016/J.JKSUCI.2021.01.007. Jan.
[134] Karkra S, Singh P, Kaur K. Convolution neural network: a shallow dive in to deep neural net technology. Int J Recent Technol Eng 2019;8(2 Special Issue 7):487–95. https://doi.org/10.35940/ijrte.B1092.0782S719.
[135] Ranschaert ER, Morozov S, Algra PR. Artificial intelligence in medical imaging: opportunities, applications and risks. Artif Intell Med Imaging Oppor Appl Risks Jan. 2019:1–373. https://doi.org/10.1007/978-3-319-94878-2.
[136] Tsang G, Xie X, Zhou SM. Harnessing the power of machine learning in dementia informatics research: issues, opportunities, and challenges. IEEE Rev Biomed Eng 2020;13:113–29. https://doi.org/10.1109/RBME.2019.2904488.
[137] Haryanto T, Suhartanto H, Murni A, Kusmardi K. Strategies to improve performance of convolutional neural network on histopathological images classification. In: 2019 International Conference on advanced computer science and information systems (ICACSIS); Oct. 2019. p. 125–32. https://doi.org/10.1109/ICACSIS47736.2019.8979740.
[138] Das A, Rad P, Choo K-KR, Nouhi B, Lish J, Martel J. Distributed machine learning cloud teleophthalmology IoT for predicting AMD disease progression. Future Generat Comput Syst Apr. 2019;93:486–98. https://doi.org/10.1016/j.future.2018.10.050.
[139] Nogales A, García-Tejedor ÁJ, Monge D, Vara JS, Antón C. A survey of deep learning models in medical therapeutic areas. Artif Intell Med Feb. 2021;112:102020. https://doi.org/10.1016/J.ARTMED.2021.102020.
[140] Li S, et al. Computer-aided assessment of breast density: comparison of supervised deep learning and feature-based statistical learning. Phys Med Biol Jan. 2018;63(2):25005. https://doi.org/10.1088/1361-6560/AA9F87.
[141] Carneiro G, Nascimento JC, Freitas A. The segmentation of the left ventricle of the heart from ultrasound data using deep learning architectures and derivative-based search methods. IEEE Trans Image Process Mar. 2012;21(3):968–82. https://doi.org/10.1109/TIP.2011.2169273.
[142] Xue Y, Zhang R, Deng Y, Chen K, Jiang T. A preliminary examination of the diagnostic value of deep learning in hip osteoarthritis. PLoS One Jun. 2017;12(6):e0178992. https://doi.org/10.1371/JOURNAL.PONE.0178992.
[143] Zhang C, et al. Hybrid adversarial-discriminative network for leukocyte classification in leukemia. Med Phys Aug. 2020;47(8):3732–44. https://doi.org/10.1002/MP.14144.
[144] Saltz J, et al. Spatial organization and molecular correlation of tumor-infiltrating Lymphocytes using deep learning on pathology images. Cell Rep Apr. 2018;23(1):181–93. https://doi.org/10.1016/J.CELREP.2018.03.086. e7.
[145] Salvi M, et al. Karpinski score under digital investigation: a fully automated segmentation algorithm to identify vascular and stromal injury of donors' kidneys. Electron Oct. 2020;9(10):1644. https://doi.org/10.3390/ELECTRONICS9101644. 2020.
[146] Chen C-M, Huang Y-S, Fang P-W, Liang C-W, Chang R-F. A computer-aided diagnosis system for differentiation and delineation of malignant regions on whole-slide prostate histopathology image using spatial statistics and multidimensional DenseNet. Med Phys 2020;47(3):1021–33. https://doi.org/10.1002/MP.13964. Mar.
[147] Fu H, et al. Disc-Aware ensemble network for glaucoma screening from fundus image. IEEE Trans Med Imag Nov. 2018;37(11):2493–501. https://doi.org/10.1109/TMI.2018.2837012.
[148] Quellec G, Charrière K, Boudi Y, Cochener B, Lamard M. Deep image mining for diabetic retinopathy screening. Med Image Anal Jul. 2017;39:178–93. https://doi.org/10.1016/J.MEDIA.2017.04.012.
[149] Saha SK, Fernando B, Cuadros J, Xiao D, Kanagasingam Y. Automated quality assessment of colour fundus images for diabetic retinopathy screening in telemedicine. J Digit Imag Apr. 2018;31(6):869–78. https://doi.org/10.1007/S10278-018-0084-9. 2018 316.
[150] Kim YD, et al. Effects of hypertension, diabetes, and smoking on age and sex prediction from retinal fundus images. Sci Rep Dec. 2020;10(1):4623. https://doi.org/10.1038/s41598-020-61519-9.
[151] Betancur J, et al. Deep learning for prediction of obstructive disease from fast myocardial perfusion SPECT: a multicenter study. JACC Cardiovasc. Imaging Nov. 2018;11(11):1654–63. https://doi.org/10.1016/J.JCMG.2018.01.020.
[152] Chaudhari AS, et al. Super-resolution musculoskeletal MRI using deep learning. Magn Reson Med Nov. 2018;80(5):2139–54. https://doi.org/10.1002/MRM.27178.
[153] Ning Z, et al. Pattern classification for gastrointestinal stromal tumors by integration of radiomics and deep convolutional features. IEEE J Biomed Heal Informatics May 2019;23(3):1181–91. https://doi.org/10.1109/JBHI.2018.2841992.
[154] Khosravan N, Celik H, Turkbey B, Jones EC, Wood B, Bagci U. A collaborative computer aided diagnosis (C-CAD) system with eye-tracking, sparse attentional model, and deep learning. Med Image Anal Jan. 2019;51:101–15. https://doi.org/10.1016/J.MEDIA.2018.10.010.
[155] 'Shin H-C, Lu L, Kim L, Seff A, Yao JH, Summers RM. Interleaved text/image deep mining on a large-scale radiology database for automated image interpretation. J Mach Learn Res 2016;17:1–31. References - Scientific Research Publishing', https://www.scirp.org/reference/referencespapers.aspx?referenceid=3014484. [Accessed 7 August 2021].
[156] Ryoungwoo, et al. Assessment of the robustness of convolutional neural networks in labeling noise by using chest X-ray images from multiple centers. JMIR Med Inf 2020;8(8):e18089. https://doi.org/10.2196/18089. 8, 8, Aug. 2020, https://medinform.jmir.org/2020/8/e18089.

[157] Cheng J-Z, et al. Computer-Aided diagnosis with deep learning architecture: applications to breast lesions in US images and pulmonary nodules in CT scans. Sci Rep Apr. 2016;6(1):1–13. https://doi.org/10.1038/srep24454. 2016 61.
[158] S Y, et al. Computer-aided diagnosis of prostate cancer using a deep convolutional neural network from multiparametric MRI. J Magn Reson Imag Dec. 2018;48(6): 1570–7. https://doi.org/10.1002/JMRI.26047.
[159] Liu Y, et al. CBCT-based synthetic CT generation using deep-attention cycleGAN for pancreatic adaptive radiotherapy. Med Phys Jun. 2020;47(6):2472–83. https://doi.org/10.1002/MP.14121.
[160] Sujit SJ, Coronado I, Kamali A, Narayana PA, Gabr RE. Automated image quality evaluation of structural brain MRI using an ensemble of deep learning networks. J Magn Reson Imag Oct. 2019;50(4):1260–7. https://doi.org/10.1002/JMRI.26693.
[161] Tang Y, Wang X, Harrison AP, Lu L, Xiao J, Summers RM. Attention-guided curriculum learning for weakly supervised classification and localization of thoracic diseases on chest radiographs. In: Lecture Notes in computer science (including subseries lecture Notes in artificial Intelligence and lecture Notes in bioinformatics). 11046. LNCS; 2018. p. 249–58.
[162] Luca AR, et al. The use of artificial intelligence on colposcopy images, in the diagnosis and staging of cervical precancers: a study protocol for a randomized controlled trial. J Biomed Sci Eng 2021;14(6):266–70. https://doi.org/10.4236/jbise.2021.146022.
[163] Ursuleanu TF, et al. The use of artificial intelligence on segmental volumes, constructed from MRI and CT images, in the diagnosis and staging of cervical cancers and thyroid cancers: a study protocol for a randomized controlled trial. J Biomed Sci Eng 2021;14(6):300–4. https://doi.org/10.4236/jbise.2021.146025.
[164] Piccialli F, Di Somma V, Giampaolo F, Cuomo S, Fortino G. A survey on deep learning in medicine: why, how and when? Inf Fusion Feb. 2021;66:111–37. https://doi.org/10.1016/J.INFFUS.2020.09.006.
[165] Alzubaidi L, et al. Towards a better understanding of transfer learning for medical imaging: a case study. Appl Sci Jun. 2020;10(13):4523. https://doi.org/10.3390/app10134523.
[166] Alzubaidi L, et al. Novel transfer learning approach for medical imaging with limited labeled data. Cancers Mar. 2021;13(7):1590. https://doi.org/10.3390/cancers13071590.
[167] Goodfellow IJ, et al. Generative Adversarial Networks. Commun ACM Jun. 2014; 63(11):139–44. Aug. 05, 2021. [Online]. Available: https://arxiv.org/abs/1406.2661v1.
[168] Hoffman J, et al. CyCADA: Cycle-Consistent adversarial domain adaptation. PMLR; Jul. 03, 2018. p. 1989–98. Aug. 07, 2021. [Online]. Available: http://proceedings.mlr.press/v80/hoffman18a.html.
[169] Long M, Zhu H, Wang J, Jordan MI. Unsupervised domain adaptation with residual transfer networks. Adv Neural Inf Process Syst Feb. 2016:136–44 [Online]. Available: http://arxiv.org/abs/1602.04433.
[170] Tzeng E, Hoffman J, Saenko K, Darrell T. Adversarial discriminative domain adaptation. In: 2017 IEEE Conference on computer vision and pattern recognition (CVPR); Jul. 2017. p. 2962–71. https://doi.org/10.1109/CVPR.2017.316.
[171] Luo Y, Zheng L, Guan T, Yu J, Yang Y. Taking a closer look at domain shift: category-level adversaries for semantics consistent domain adaptation. IEEE Comput Soc Conf Comput Vis Pattern Recogn Jun. 2019;2019-June:2502–11. https://doi.org/10.1109/CVPR.2019.00261.
[172] Tsai Y-H, Hung W-C, Schulter S, Sohn K, Yang M-H, Chandraker M. Learning to adapt structured output space for semantic segmentation. In: 2018 IEEE/CVF Conference on computer vision and pattern recognition; Jun. 2018. p. 7472–81. https://doi.org/10.1109/CVPR.2018.00780.
[173] Liu D, et al. PDAM: a panoptic-level feature alignment framework for unsupervised domain adaptive instance segmentation in microscopy images. IEEE Trans Med Imag Jan. 2021;40(1):154–65. https://doi.org/10.1109/TMI.2020.3023466.
[174] Ghafoorian M, et al. Transfer learning for domain adaptation in MRI: application in brain lesion segmentation. Lect Notes Comput Sci (including Subser Lect Notes Artif Intell Lect Notes Bioinformatics) Sep. 2017;10435:516–24. https://doi.org/10.1007/978-3-319-66179-7_59. LNCS.
[175] Jiang J, et al. Tumor-Aware, adversarial domain adaptation from CT to MRI for lung cancer segmentation. Lect Notes Comput Sci (including Subser Lect Notes Artif Intell Lect Notes Bioinformatics) Sep. 2018;11071:777–85. https://doi.org/10.1007/978-3-030-00934-2_86. LNCS.
[176] Chen C, Dou Q, Chen H, Heng PA. Semantic-aware generative adversarial nets for unsupervised domain adaptation in chest X-ray segmentation. Lect Notes Comput Sci 2018;11046:143–51. LNCS.
[177] Yang J, Dvornek NC, Zhang F, Chapiro J, De Lin M, Duncan JS. Unsupervised domain adaptation via disentangled representations: application to cross-modality liver segmentation. Lect Notes Comput Sci 2019;11765:255–63. LNCS.
[178] Li CY, Liang X, Hu Z, Xing EP. Knowledge-Driven encode, retrieve, paraphrase for medical image report generation. Proc AAAI Conf Artif Intell Jul. 2019;33(1): 6666–73. https://doi.org/10.1609/AAAI.V33I01.33016666.
[179] Wang Z, Zhang J, Feng J, Chen Z. Knowledge graph and text jointly embedding. EMNLP 2014 - 2014 Conf. Empir Methods Nat Lang Process Proc Conf 2014: 1591–601. https://doi.org/10.3115/V1/D14-1167.
[180] Luo B, Shen J, Cheng S, Wang Y, Pantic M. 'Shape Constrained network for eye segmentation in the Wild', *proc. - 2020 IEEE Winter Conf.* Appl. Comput. Vision, WACV 2020. Oct. 2019. p. 1941–9. Aug. 05, 2021. [Online]. Available: https://arxiv.org/abs/1910.05283v1.
[181] Wistuba M, Rawat A, Pedapati T. A survey on neural architecture search. May 2019. Jul. 30, 2021. [Online]. Available: http://arxiv.org/abs/1905.01392.
[182] Guo D, et al. Organ at risk segmentation for head and neck cancer using stratified learning and neural architecture search. IEEE Comput Soc Conf Comput Vis Pattern Recogn 2020:4222–31. https://doi.org/10.1109/CVPR42600.2020.00428.